

Two dimensional mortar contact methods for large deformation frictional sliding

Bin Yang, Tod A. Laursen^{*,†} and Xiaonong Meng[‡]

*Department of Civil and Environmental Engineering, Computational Mechanics Laboratory,
Duke University, Durham, NC 27708-0287, U.S.A.*

SUMMARY

This paper presents a mortar-based formulation for the solution of two dimensional frictional contact problems involving finite deformation and large sliding. As is widely recognized, traditional node-to-surface contact formulations have several drawbacks in solution of deformable-to-deformable contact problems, including lack of general patch test passage, degradation of spatial convergence rates, and robustness issues associated with the faceted representation of contacting surfaces. The mortar finite element method, initially proposed as a technique to join dissimilarly meshed domains, has been shown to preserve optimal convergence rates in tied contact problems (see (*Discretization Methods and Iterative Solvers Based on Domain Decomposition*, Springer-Verlag, Heidelberg, 2001) for a recent review), and is examined here as an alternative spatial discretization method for large sliding contact. In particular, a novel description for frictional sliding conditions in large deformation mortar formulations is proposed in this work.

In recent years, the mortar element method has already been successfully implemented to solve frictional contact problems with linearized kinematics (see (*Int. J. Numer. Meth. Engng* 1993; **36**: 3451)). However, in the presence of large deformations and finite sliding, one must face difficulties associated with the definition and linearization of contact virtual work in the case where the mortar projection has a direct dependence on the tangential relative motion along the interface. In this paper, such a formulation is presented, with particular emphasis on key aspects of the linearization procedure and on the robust description of the friction kinematics. Some novel techniques are proposed to treat the non-smoothness in the contact geometry and the searching required to define mortar segments. A number of numerical examples illustrate the performance and accuracy of the proposed formulation. Copyright © 2004 John Wiley & Sons, Ltd.

KEY WORDS: friction; mortar methods; contact; large sliding; finite elements

^{*}Correspondence to: T. A. Laursen, Department of Civil and Environmental Engineering, Computational Mechanics Laboratory, Duke University, Durham, NC 27708-0287, U.S.A.

[†]E-mail: laursen@duke.edu

[‡]Current Address: Abaqus, Inc., 1080 Main Street, Pawtucket, RI 02860, U.S.A.

Contract/grant sponsor: Air Force office of Scientific Research; contract/grant number: F49620-02-1-0094

Contract/grant sponsor: Sandia National Laboratories; contract/grant number: 21757

Received 3 November 2003

Revised 26 April 2004

Accepted 18 August 2004

1. INTRODUCTION

This article deals with the mortar finite element formulation of large deformation frictional sliding contact problems, which are found in many important applications in engineering and the sciences. Numerical solution of these problems is quite challenging, with robustness issues in particular arising from extreme non-linearity and non-smoothness of the contact operators, which must be handled in the presence of large deformation and significant relative sliding of the contacting bodies. In recent years, there have been significant advances in this field, with many formulations becoming available in the research literature and in commercial finite element codes. However, the robustness of these formulations is still a limitation in many problems of interest. The aim of this research is to provide a formulation which can solve general large deformation frictional contact problem in a robust, accurate and stable manner. The technique we propose for this purpose, a *mortar formulation* of the contact conditions, employs an integral projection of contact variables on the contact surface to provide a consistent representation of all contact variables over a single discretization. The approach presented here represents a penalty regularization of the classical mortar approaches to be found (for example) in Reference [1] or Reference [2], although it should be emphasized also that there is nothing from an algorithmic point of view which precludes use of Lagrange multiplier or augmented Lagrangian strategies for enforcement of the contact constraints formulated herein. The procedures needed to set up the mortar formulation of the problem, to linearize the mortar contact virtual work, and assemble the contact stiffness are discussed in detail in this paper. In particular, the description of large sliding frictional mortar contact formulations, given in this paper in a two dimensional context, is to our knowledge unprecedented.

The most prevalent finite element formulations dealing with large deformation contact problems are based on the so called master/slave contact strategies [3–5], in which the nodes of one deformable surface (the slave surface) are prohibited from penetrating the element boundaries of the opposing surface (the master surface). This approach represents a collocation method with the physical requirement of impenetrability being enforced at these points (usually taken to be the nodes). However, as indicated by Papadopoulos and Taylor [6], the master/slave contact strategies are not guaranteed to pass contact patch tests, wherein a flat contact surface should be able to transmit a spatially constant contact pressure from one body to the other. The issue of patch test passage (or lack thereof) could be expected to relate directly to the numerical convergence performance of contact formulations [7]; the degraded convergence of such node-to-surface formulations has in fact been demonstrated in a kinematically linear context by Hild [8]. Another shortcoming of the node-to-surface formulation is the non-smoothness of the discretized contact surfaces. To monitor the motion of material points with respect to the master surface, slave points need to be projected onto the discretized master surface. Such projections are frequently problematic where element boundaries meet to form edges and corners, because there the surface normal is discontinuous and convergence difficulties (as well as non-physical oscillations) tend to result.

The mortar element method (see, e.g., References [1, 2, 9, 10]) was originally introduced as a domain decomposition method, used to couple possibly nonconforming discretizations across subdomain boundaries. For example, early implementations of the mortar element method were used in conjunction with spectral methods (see Reference [11]). The mortar method introduces the continuity condition at interfaces in integral (global) form, rather than as nodal (local) constraints. One of the significant advantages of the mortar finite element method is that

it preserves optimal convergence rates from the finite element methods (see Reference [1]) provided suitable mortar spaces are chosen. Since such suitable spaces can be shown to satisfy appropriate inf-sup conditions for the method, we have the significant advantage that the mortar method satisfies Babuska–Brezzi stability conditions as well.

These advantages make the mortar element method a very promising candidate for application to contact problems. Contact constraints can be readily expressed in integral form by introducing a mortar space on one or both of the contact surfaces. In this way, mortar element methods have been successfully applied to contact problems with infinitesimal deformation. Belgacem *et al.* [12, 13] first analysed unilateral frictional contact problems with a mortar finite element method. McDevitt and Laursen [14] incorporated Coulomb frictional behaviour in their mortar contact formulation and introduced an intermediate contact surface to facilitate the evaluation of the contact integrals. Penalty regularization was used to apply the normal and tangential contact constraints in their formulation. Krause and Wohlmuth [15] implemented a Dirichlet–Neumann type of algorithm to solve frictional contact problems, using a mortar element method based on a dual basis Lagrange multiplier space. They used monotone multigrid methods to solve the global equations. Hild [8] compared the mortar element method and node-to-surface strategy for frictionless contact problems, and numerically demonstrated optimality of the mortar formulation (and lack of optimality for its node-to-surface counterpart).

Although large deformation formulation of contact problems based on node-to-surface strategies has been commonplace for quite some time (see, e.g., References [16, 17] and the recent monograph [7]), efforts in the literature to generally treat large deformation contact problems using mortar element methods have not appeared until very recently [18]. As is discussed in detail for the three dimensional frictionless case in Reference [18], mortar element formulation of large deformation/sliding contact problems is difficult because the mortar integrals and associated surface-to-surface projections are strongly dependent on the deformation of the contact bodies. This requires that the terms in the contact virtual work related to the deformation of the contact bodies are properly linearized; the stiffness emanating from those terms arising from the (changing) mortar projection is particularly intricate (and crucial) to obtain. Furthermore, the faceted nature of the contact surfaces introduces difficulties associated with ‘corners’ when conducting mortar searching, which if handled inappropriately will result in poor convergence performance of the method.

In this paper, a mortar formulation for large deformation frictional contact problems is implemented, working in the context of two dimensional problems in solid mechanics. For the first time, frictional response is included in a large deformation, finite sliding mortar contact method. The formulation includes a novel technique for defining a continuous normal field on the discretized contact surface, which is used for searching and definition of the mortar segments that are used to compute the requisite mortar projections. A detailed procedure of linearization of the contact virtual work is given, such that a Newton–Raphson iterative solver can be applied. Several numerical benchmarks examples are computed to demonstrate the robustness and accuracy of the method, and to emphasize its advantages over existing approaches.

2. PROBLEM DESCRIPTION

A two dimensional contact problem, with large deformation and large sliding, is shown in Figure 1. As shown in the figure, the reference configurations of two contacting bodies are

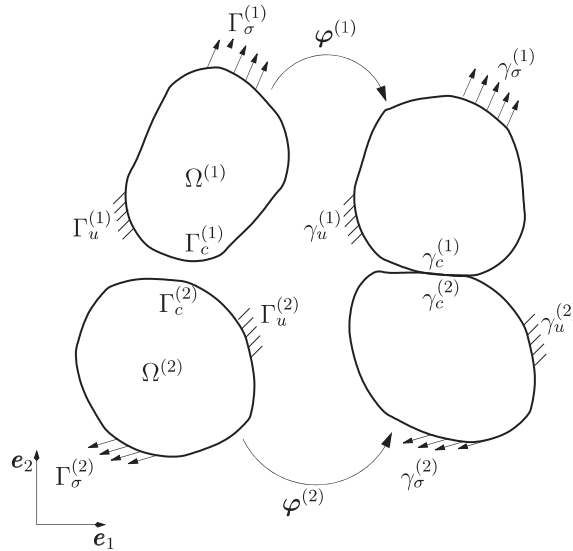


Figure 1. Notation for the two body large deformation contact problem.

represented by the open sets $\Omega^{(1)}$ and $\Omega^{(2)}$. The deformation mappings of the two bodies are denoted by $\varphi^{(1)}$ and $\varphi^{(2)}$, respectively. The closure of $\Omega^{(i)}$, $i = 1, 2$ will be denoted as $\bar{\Omega}^{(i)}$, and is the union of the open set with its boundary $\partial\Omega^{(i)}$.

The surfaces $\partial\Omega^{(i)}$ are divided into $\Gamma_u^{(i)}$, where displacements are prescribed; $\Gamma_\sigma^{(i)}$, where tractions are prescribed; and $\Gamma_c^{(i)}$, where the contact constraints will be defined. In keeping with a common nomenclature, we will denote $\Gamma_c^{(1)}$ and $\Gamma_c^{(2)}$ as the slave and master surfaces, respectively, although these terminologies will not retain their same meanings as in traditional strategies. The spatial counterparts of these three portions are denoted by $\gamma_u^{(i)}$, $\gamma_\sigma^{(i)}$ and $\gamma_c^{(i)}$, respectively. We assume $\Gamma_u^{(i)}$, $\Gamma_\sigma^{(i)}$ and $\Gamma_c^{(i)}$ satisfy

$$\Gamma_u^{(i)} \cup \Gamma_\sigma^{(i)} \cup \Gamma_c^{(i)} = \partial\Omega^{(i)} \quad (1)$$

and

$$\Gamma_\sigma^{(i)} \cap \Gamma_u^{(i)} = \Gamma_\sigma^{(i)} \cap \Gamma_c^{(i)} = \Gamma_u^{(i)} \cap \Gamma_c^{(i)} = \emptyset \quad (2)$$

for each of the bodies (i). Traction and motion boundary conditions are stated in the standard manner (with respect to the reference configuration) as

$$\begin{aligned} P_{jJ}^{(i)} N_J^{(i)} &= \bar{T}_j^{(i)} \quad \text{in } \Gamma_\sigma^{(i)} \\ \varphi_j^{(i)} &= \bar{\varphi}_j^{(i)} \quad \text{in } \Gamma_u^{(i)} \end{aligned} \quad (3)$$

where $\bar{T}_i^{(i)}$ and $\bar{u}_i^{(i)}$ denote the prescribed tractions and displacements associated with body (i) , $N_j^{(i)}$ is the component of the outward normal to $\partial\Gamma_\sigma^{(i)}$ in the reference configuration, and $P_{jj}^{(i)}$ denotes the components of the first Piola–Kirchhoff stress tensor in body (i) .

To define the virtual work, we first define solution and weighting spaces $\mathcal{C}^{(i)}$ and $\mathcal{V}^{(i)}$, consisting of solutions $\boldsymbol{\varphi}^{(i)}$ and their variations $\boldsymbol{\Phi}^{(i)}$ according to

$$\mathcal{C}^{(i)} = \left\{ \boldsymbol{\varphi}^{(i)} : \bar{\Omega}^{(i)} \rightarrow \mathbb{R}^2 \mid \boldsymbol{\varphi}^{(i)} \in H^1(\Omega^{(i)}), \boldsymbol{\varphi}^{(i)} = \bar{\boldsymbol{\varphi}}^{(i)} \text{ in } \Gamma_u^{(i)} \right\} \quad (4)$$

and

$$\mathcal{V}^{(i)} = \left\{ \boldsymbol{\Phi}^{(i)} : \bar{\Omega}^{(i)} \rightarrow \mathbb{R}^2 \mid \boldsymbol{\Phi}^{(i)} \in H^1(\Omega^{(i)}), \boldsymbol{\Phi}^{(i)} = \mathbf{0} \text{ in } \Gamma_u^{(i)} \right\} \quad (5)$$

where $H^1(\Omega^{(i)})$ represents the Sobolev space of functions which have square integrable derivatives.

Given these ideas, the virtual work principle for the two body contact problem in large deformations can be written as

$$\begin{aligned} G(\boldsymbol{\varphi}, \boldsymbol{\Phi}) &:= \sum_{i=1}^2 G^{(i)}(\boldsymbol{\varphi}^{(i)}, \boldsymbol{\Phi}^{(i)}) \\ &= \sum_{i=1}^2 \left\{ \int_{\Omega^{(i)}} \left[\rho_0^{(i)} \boldsymbol{\Phi}^{(i)} \cdot \mathbf{A}^{(i)} + \text{Grad } \boldsymbol{\Phi}^{(i)} : \mathbf{P}^{(i)} \right] d\Omega \right. \\ &\quad \left. - \int_{\Omega^{(i)}} \boldsymbol{\Phi}^{(i)} \cdot \mathbf{F}^{(i)} d\Omega - \int_{\Gamma_\sigma^{(i)}} \boldsymbol{\Phi}^{(i)} \cdot \bar{\mathbf{T}}^{(i)} d\Gamma \right\} \\ &\quad - \sum_{i=1}^2 \int_{\Gamma_c^{(i)}} \boldsymbol{\Phi}^{(i)} \cdot \mathbf{t}^{(i)} d\Gamma = 0 \\ &= G^{\text{int,ext}}(\boldsymbol{\varphi}, \boldsymbol{\Phi}) + G^c(\boldsymbol{\varphi}, \boldsymbol{\Phi}) = 0 \end{aligned} \quad (6)$$

In (6), $G^{\text{int,ext}}(\boldsymbol{\varphi}, \boldsymbol{\Phi})$ is the sum of the virtual work arising from the internal and external forces, while the notation $G^c(\boldsymbol{\varphi}, \boldsymbol{\Phi})$ denotes the virtual work associated with the contact tractions. The notation $\mathbf{A}^{(i)}$ has been employed to denote the material acceleration field in body (i) (in the event that inertial effects are present), $\rho_0^{(i)}$ denotes the reference density, and $\mathbf{F}^{(i)}$ denotes the body force in body (i) .

In our mortar contact implementation, we represent the contact virtual work in the current configuration as

$$\begin{aligned} G^c(\boldsymbol{\varphi}, \boldsymbol{\Phi}) &= - \sum_{i=1}^2 \int_{\Gamma_c^{(i)}} \boldsymbol{\Phi}^{(i)} \cdot \mathbf{t}^{(i)} d\Gamma \\ &= - \sum_{i=1}^2 \int_{\gamma_c^{(i)}} \boldsymbol{\Phi}^{(i)} \cdot \boldsymbol{\lambda}^{(i)} d\gamma \end{aligned} \quad (7)$$

where $\gamma_c^{(i)}$ is the current configuration of the contact surface on body (i), and the mortar multiplier $\lambda^{(i)}$ denotes the Cauchy contact traction. Once the balance of linear momentum across the contact interface is considered, we have

$$\lambda^{(1)} d\gamma_c^{(1)} = -\lambda^{(2)} d\gamma_c^{(2)} \quad (8)$$

which implies that the contact virtual work in (7) can be replaced by

$$G^c(\boldsymbol{\varphi}, \boldsymbol{\Phi}^*) := - \int_{\gamma_c^{(1)}} \lambda^{(1)}(\mathbf{X}) \cdot (\boldsymbol{\Phi}^{*(1)}(\mathbf{X}) - \boldsymbol{\Phi}^{*(2)}(\bar{\mathbf{Y}})) d\gamma \quad (9)$$

where $\boldsymbol{\Phi}^{(2)}(\bar{\mathbf{Y}})$ is the current position of the contact point for \mathbf{X} . It is important to note that while in a node to surface method, $\bar{\mathbf{Y}}$ would be determined for each (nodal) point \mathbf{X} via closest point projection, here we employ a spatial integration procedure which will indirectly identify pairings between points \mathbf{X} and $\bar{\mathbf{Y}}$. To draw the correspondence with the mortar literature, the slave surface $\gamma_c^{(1)}$ is referred to as the *non-mortar* surface, as it is the one where the Lagrange multipliers will be interpolated, while the master surface $\gamma_c^{(2)}$ is called the *mortar* surface.

3. CONTACT KINEMATICS AND CONSTRAINTS

3.1. Normal contact conditions

The normal contact constraints enforce the physical requirements of impenetrability and compressive interaction between contact bodies. We define the gap function $g(\mathbf{X}, t)$ as

$$g(\mathbf{X}, t) = \mathbf{n} \cdot [\boldsymbol{\Phi}^{(1)}(\mathbf{X}, t) - \boldsymbol{\Phi}^{(2)}(\bar{\mathbf{Y}}, t)] \quad (10)$$

where $\bar{\mathbf{Y}}$ denotes the (material) contact point for \mathbf{X} at time t , and \mathbf{n} denotes the outward unit normal to $\gamma_c^{(1)}$ at $\mathbf{x} = \boldsymbol{\Phi}^{(1)}(\mathbf{X}, t)$. The condition of impenetrability for the material point \mathbf{X} relative to the master surface can be represented as

$$g(\mathbf{X}, t) \leq 0 \quad (11)$$

The gap function and contact pressure (normal component of the contact traction) are interrelated through the remainder of the classical Kuhn–Tucker conditions:

$$\lambda_N(\mathbf{X}, t) \geq 0 \quad (12)$$

and

$$\lambda_N(\mathbf{X}, t) g(\mathbf{X}, t) = 0 \quad (13)$$

where $\lambda_N(\mathbf{X}, t) = -\boldsymbol{\lambda} \cdot \mathbf{n}$ is the Cauchy contact pressure at material point \mathbf{X} on the slave surface. Equation (12) implies that only compressive interaction is allowed, while (13) allows the contact pressure to be non-zero only when $g(\mathbf{X}, t) = 0$.

3.2. Frictional contact conditions

To characterize the frictional response, we define the relative velocity as the summation of normal and tangential components as

$$\begin{aligned}\mathbf{v} &= \dot{\boldsymbol{\phi}}^{(2)}(\bar{\mathbf{Y}}, t) - \dot{\boldsymbol{\phi}}^{(1)}(\mathbf{X}, t) \\ &= \mathbf{v}_N + \mathbf{v}_T = v_N \mathbf{n} + v_T \boldsymbol{\tau}\end{aligned}\quad (14)$$

where $\boldsymbol{\tau}$ is the unit tangential vector defined in the current configuration of the slave surface as

$$\boldsymbol{\tau} = \mathbf{e}_3 \times \mathbf{n} \quad (15)$$

where \mathbf{e}_3 is the unit basis vector pointing out of the paper. As has been widely recognized for some time (see, e.g. Reference [7]), use of the above v_T in finite deformation formulations of frictional response is *only frame indifferent in the event that $g = 0$ at the point where v_T is being evaluated*; otherwise, an algorithmic modification of this slip rate is necessary. We shall discuss an appropriate adaptation of that modification for the mortar formulation of friction in the next section.

The contact traction $\boldsymbol{\lambda} = \boldsymbol{\lambda}^{(1)} = -\boldsymbol{\lambda}^{(2)}$ can also be resolved into normal and tangential components as:

$$\begin{aligned}\boldsymbol{\lambda} &= \lambda_N + \lambda_T \\ &= -\lambda_N \mathbf{n} + \lambda_T \boldsymbol{\tau}\end{aligned}\quad (16)$$

With these notions in hand, the conditions for Coulomb friction can be written as

$$\mathbf{v}_T - \dot{\gamma} \frac{\boldsymbol{\lambda}_T}{\|\boldsymbol{\lambda}_T\|} = \mathbf{0} \quad (17)$$

$$\Phi := \|\boldsymbol{\lambda}_T\| - \mu \|\lambda_N\| \leq 0 \quad (18)$$

$$\dot{\gamma} \geq 0 \quad (19)$$

$$\Phi \dot{\gamma} = 0 \quad (20)$$

where, as can be seen, the frictional traction is forced to oppose the tangential velocity (note the sign change inherent to the definition of tangential velocity in Equation (14)).

4. DISCRETIZATION OF FRICTIONAL CONTACT WITH THE MORTAR ELEMENT METHOD

As mentioned in the introduction, the mortar element method is used in general to weakly couple fields between potentially mismatched surfaces. Application of this method in the current context has been shown to preserve optimal convergence rates in tied contact problems [2] and

is examined here as an alternative spatial discretization method for large sliding frictional contact problems.

In this paper, we use two dimensional bilinear finite elements to spatially discretize the contacting bodies, and consider the mortar approximations that should be used on the interface to describe the contact of these bodies—the approach can be extended for use with quadratic and higher order elements without conceptual difficulty. Consider the spatial discretization of bodies $\Omega^{(i)}$ using the finite set of elements $\mathcal{E}^{(i)h}$:

$$\Omega^{(i)h} = \bigcup_{e \in \mathcal{E}^{(i)h}} \Omega_e^{(i)} \quad (21)$$

The discretization of contact surfaces $\Gamma_c^{(i)h}$ occurs over subsets of $\partial\Omega^{(i)h}$.

Finite dimensional subspaces of solution and weighting spaces in (4) and (5) are denoted $\mathcal{C}^{(i)h}$ and $\mathcal{V}^{(i)h}$, and may be defined via

$$\begin{aligned} \mathcal{C}^{(i)h} = \left\{ \boldsymbol{\varphi}^{(i)h} : \bar{\Omega}^{(i)h} \rightarrow \mathbb{R}^2 \mid \boldsymbol{\varphi}^{(i)h} \in C^0(\Omega^{(i)h}) \right. \\ \left. \forall e \in \mathcal{E}^{(i)h}, \boldsymbol{\varphi}^{(i)h}(\Omega_e^{(i)h}) \in \mathbb{P}_N(\Omega_e^{(i)h}); \boldsymbol{\varphi}^{(i)h} = \bar{\boldsymbol{\varphi}}^{(i)} \text{ in } \Gamma_u^{(i)h} \right\} \end{aligned} \quad (22)$$

and

$$\begin{aligned} \mathcal{V}^{(i)h} = \left\{ \boldsymbol{\Phi}^{*(i)h} : \bar{\Omega}^{(i)h} \rightarrow \mathbb{R}^2 \mid \boldsymbol{\Phi}^{*(i)h} \in C^0(\Omega^{(i)h}) \right. \\ \left. \forall e \in \mathcal{E}^{(i)h}, \boldsymbol{\Phi}^{*(i)h}(\Omega_e^{(i)h}) \in \mathbb{P}_N(\Omega_e^{(i)h}); \boldsymbol{\Phi}^{*(i)h} = \mathbf{0} \text{ in } \Gamma_u^{(i)h} \right\} \end{aligned} \quad (23)$$

where $\mathbb{P}_N(\Omega_e^{(i)h})$ is the set of all polynomials on $\Omega_e^{(i)h}$ of order $\leq N$. The mortar and non-mortar fields, $\boldsymbol{\varphi}^{(i)h}(\Gamma_c^{(i)h}) \subset \mathcal{X}^{(i)h}$, and the variations of these fields, $\boldsymbol{\Phi}^{*(i)h}(\Gamma_c^{(i)h}) \subset \mathcal{W}^{(i)h}$, are subsets of $\mathcal{C}^{(i)h}$ and $\mathcal{V}^{(i)h}$ and are obtained by restriction of (22) and (23) to contact surfaces $\Gamma_c^{(i)h}$. The discretized mortar multiplier space, which is physically interpreted as the space containing contact tractions, is defined on the non-mortar side (i.e. slave surface) as

$$\mathcal{M}^h = \left\{ \boldsymbol{\lambda}^h \mid \boldsymbol{\lambda}^h \in C^0(\Gamma_c^{(1)h}); \forall e \in \mathcal{P}^h, \boldsymbol{\lambda}^h(\Gamma_{c_e}^{(1)h}) \in \mathbb{P}_N(\Gamma_{c_e}^{(1)h}) \right\} \quad (24)$$

where \mathcal{P}^h is the set of non-mortar element edges making up the slave surface.

With these definitions in hand, we may now define the discretized version of contact virtual work by developing shape function expansions for the above contact surface fields and substituting into (9). The discretized multipliers, the deformation fields and their variations on the contact surface may be interpolated as

$$\boldsymbol{\lambda}^h(\mathbf{X}) = \sum_{A=1}^{n_s} N_A^{(1)}(\boldsymbol{\zeta}^{(1)}(\mathbf{X})) \boldsymbol{\lambda}_A \quad (25)$$

$$\boldsymbol{\varphi}^{(1)h}(\mathbf{X}) = \sum_{D=1}^{n_s} N_D^{(1)}(\boldsymbol{\xi}^{(1)}(\mathbf{X})) \boldsymbol{\varphi}_D^{(1)} \quad (26)$$

$$\boldsymbol{\varphi}^{(2)h}(\bar{\mathbf{Y}}) = \sum_{E=1}^{n_m} N_E^{(2)}(\boldsymbol{\xi}^{(2)}(\bar{\mathbf{Y}})) \boldsymbol{\varphi}_E^{(2)} \quad (27)$$

$$\boldsymbol{\Phi}^{*(1)h}(\mathbf{X}) = \sum_{B=1}^{n_s} N_B^{(1)}(\boldsymbol{\xi}^{(1)}(\mathbf{X})) \boldsymbol{\Phi}_B^{*(1)} \quad (28)$$

$$\boldsymbol{\Phi}^{*(2)h}(\bar{\mathbf{Y}}) = \sum_{C=1}^{n_m} N_C^{(2)}(\boldsymbol{\xi}^{(2)}(\bar{\mathbf{Y}})) \boldsymbol{\Phi}_C^{*(2)} \quad (29)$$

where A , B and D are indices associated with slave (non-mortar) nodes, and C and E are indices associated with master (mortar) nodes. All shape functions $N_{\bullet}^{(i)}$ denote the restriction of the finite element shape functions associated with either body (1) or (2) to the appropriate contact boundary. Other notations in (25)–(29) include λ_A for the nodal values of contact tractions at slave nodes; $\boldsymbol{\Phi}_B^{*(1)}$ and $\boldsymbol{\Phi}_C^{*(2)}$ for nodal values of $\boldsymbol{\Phi}^{*(1)h}$ and $\boldsymbol{\Phi}^{*(2)h}$; and $\boldsymbol{\varphi}_D^{(1)}$ and $\boldsymbol{\varphi}_E^{(2)}$ for nodal values of $\boldsymbol{\varphi}^{(1)h}$ and $\boldsymbol{\varphi}^{(2)h}$. The limits on the sums, n_s and n_m , are numbers of nodes on the slave and master surfaces, respectively.

One may substitute Equations (25), (28) and (29) into (9) to obtain an expression for the mortar approximation the contact virtual work, denoted in the sequel as G^{cm} :

$$G^{\text{cm}}(\boldsymbol{\varphi}^h, \boldsymbol{\Phi}^{*h}) = - \sum_A \sum_B \sum_C \lambda_A \cdot \left[n_{AB}^{(1)} \boldsymbol{\Phi}_B^{*(1)} - n_{AC}^{(2)} \boldsymbol{\Phi}_C^{*(2)} \right] \quad (30)$$

where the expressions for the $n_{AB}^{(1)}$ and $n_{AC}^{(2)}$ are:

$$n_{AB}^{(1)} = \int_{\gamma^{(1)h}} N_A^{(1)}(\boldsymbol{\xi}^{(1)}(\mathbf{X})) N_B^{(1)}(\boldsymbol{\xi}^{(1)}(\mathbf{X})) d\gamma \quad (31)$$

$$n_{AC}^{(2)} = \int_{\gamma^{(1)h}} N_A^{(1)}(\boldsymbol{\xi}^{(1)}(\mathbf{X})) N_C^{(2)}(\boldsymbol{\xi}^{(2)}(\bar{\mathbf{Y}}(\mathbf{X}))) d\gamma \quad (32)$$

In the sequel, we will reference $n_{AB}^{(1)}$ and $n_{AC}^{(2)}$ as the mortar integrals.

The normal and tangential portions of the contact operator are now exposed by splitting λ_A into normal and frictional parts:

$$\lambda_A = \lambda_{N_A} + \lambda_{T_A} \quad (33)$$

The key to our algorithm lies in defining λ_{N_A} and λ_{T_A} in terms of the kinematics of the problem.

4.1. Definition of the normal contact constraints

As was demonstrated previously in Reference [18], the normal part of the contact traction may be represented as

$$\lambda_{N_A} = -\lambda_{N_A} \mathbf{n}_A \quad (\text{no sum}) \quad (34)$$

where λ_{N_A} represents the contact pressure at node A. It is subject to Kuhn–Tucker conditions via

$$\begin{aligned}\lambda_{N_A} &\geq 0 \\ g_A &\leq 0 \\ \lambda_{N_A} g_A &= 0\end{aligned}\tag{35}$$

where the mortar projected gap g_A at slave node A is defined as

$$\begin{aligned}g_A &= \mathbf{n}_A \cdot \mathbf{g}_A \\ \mathbf{g}_A &:= \kappa_A \left[\sum_B n_{AB}^{(1)} \boldsymbol{\Phi}_B^{(1)} - \sum_C n_{AC}^{(2)} \boldsymbol{\Phi}_C^{(2)} \right]\end{aligned}\tag{36}$$

where κ_A is a scale factor defined as

$$\begin{aligned}\kappa_A &= \frac{1}{\sum_D n_{AD}^{(1,\text{ref})}} \\ n_{AD}^{(1,\text{ref})} &= \int_{\Gamma^{(1)h}} N_A^{(1)} \left(\boldsymbol{\xi}^{(1)}(\mathbf{X}) \right) N_D^{(1)} \left(\boldsymbol{\xi}^{(1)}(\mathbf{X}) \right) d\Gamma\end{aligned}\tag{37}$$

with $\Gamma^{(1)h}$ being the original configuration of the discretized slave surface. This scaling, while not by any means unique, is performed to cause the gap function \mathbf{g}_A to have the proper units of length, which is of crucial importance when implementing penalty methods in particular. Equation (36) is written in terms of a nodal normal \mathbf{n}_A , based at the *slave node*. Definition of this normal is a crucial aspect of our algorithm and is integrally tied to the way we do the mortar searching; accordingly, further discussion of it is deferred to the next section.

Although other choices are possible, we consider here the use of penalty regularization to enforce the normal contact conditions given in (35). In this case, the normal traction at node A assumes the following form:

$$\lambda_{N_A} = -\varepsilon_N \langle g_A \rangle \mathbf{n}_A\tag{38}$$

where ε_N is the normal penalty parameter, and $\langle \bullet \rangle$ is the Macauley bracket, representing the positive part of the operand. Augmented Lagrangian treatment of the constraint, using the above penalization as a kernel, is readily done; the interested reader is referred to [7] for extensive discussion of such algorithms.

4.2. Definition of the frictional contact conditions

The first step in defining the treatment of the frictional operator is to specify a penalty regularization of conditions (17)–(20). This may be done via

$$\begin{aligned}\mathcal{L}_v \lambda_T &= \varepsilon_T \left[\mathbf{v}_T - \dot{\gamma} \frac{\lambda_T}{\|\lambda_T\|} \right] \\ \Phi &:= \|\lambda_T\| - \mu \|\lambda_N\| \leq 0 \\ \dot{\gamma} &\geq 0 \\ \Phi \dot{\gamma} &= 0\end{aligned}\tag{39}$$

where ε_T is the frictional penalty parameter. The frictional conditions (17)–(20) are recovered in the limit as $\varepsilon_T \rightarrow \infty$. $\mathcal{L}_v \lambda_T$ is the *Lie derivative* of the frictional traction, and may be defined in the current context via

$$\mathcal{L}_v \lambda_T = \dot{\lambda}_T \tau \quad (40)$$

where τ is the unit tangential base vector. Equation (40) contains material time derivatives of the components of λ_T only (i.e. no terms containing time derivatives of base vectors are present). It is fact that makes it a frame indifferent object.

We now wish to assure that the remainder of the frictional constitutive relation in (39) is frame indifferent. As was stated earlier, in the continuum mechanical case, the tangential component of the relative velocity is not frame indifferent when the gap g differs from zero. In that instance, however, frame indifference can be restored by adding in a dilatant portion to the tangential velocity measure (see Reference [7]). In the current (mortar projected) instance, we must perform a similar operation to assure frame indifference. Working in the time continuous case first, one may readily show that the tangential component of the *mortar projected* tangential velocity is not frame indifferent:

$$\mathbf{v}_{T_A}^{\text{nonobj}} := -\kappa_A \left[\sum_B n_{AB}^{(1)} \dot{\Phi}_B^{(1)} - \sum_C n_{AC}^{(2)} \dot{\Phi}_C^{(2)} \right] \cdot \tau_A \otimes \tau_A \quad (41)$$

where $\tau_A = \mathbf{e}_3 \times \mathbf{n}_A$.

Frame indifference is assessed by viewing the motion from another reference frame, denotes in the following by superscripts $*$, which can be related to the original spatial frame via:

$$\boldsymbol{\phi}^* = \mathbf{c}(t) + \mathbf{Q}(t)\boldsymbol{\phi} \quad (42)$$

In (42), $\mathbf{c}(t)$ is a relative rigid body translation between the original spatial frame and observer $*$, while a relative rotation is produced by the proper orthogonal tensor $\mathbf{Q}(t)$. The frame indifferent relative tangential velocity should satisfy

$$\mathbf{v}_{T_A}^* = \mathbf{Q}(t)\mathbf{v}_{T_A} \quad (43)$$

However, by considering the effect of the transformation (42) on (41), it is readily seen that

$$\mathbf{v}_{T_A}^{\text{nonobj}*} = \mathbf{Q}(t)\mathbf{v}_{T_A}^{\text{nonobj}} - \dot{\mathbf{Q}}(t)\kappa_A \left[\sum_B n_{AB}^{(1)} \Phi_B^{(1)} - \sum_C n_{AC}^{(2)} \Phi_C^{(2)} \right] \cdot [\mathbf{Q}\tau_A] \otimes [\mathbf{Q}\tau_A] \quad (44)$$

Because the bracketed term $[\sum_B n_{AB}^{(1)} \Phi_B^{(1)} - \sum_C n_{AC}^{(2)} \Phi_C^{(2)}] \neq \mathbf{0}$ in general, $\mathbf{v}_{T_A}^{\text{nonobj}*}$ does not satisfy Equation (43), and thus some modification is required to this relative velocity measure to assure material frame indifference.

It turns out that this objectivity is restored by inclusion of the rate of a mortar projected distance between the two bodies, denoted as \mathbf{g}_A in (36)). Namely, if we consider

$$\mathbf{v}_{T_A} := - \left[\kappa_A \left(\sum_B n_{AB}^{(1)} \dot{\Phi}_B^{(1)} - \sum_C n_{AC}^{(2)} \dot{\Phi}_C^{(2)} \right) - \dot{\mathbf{g}}_A \right] \cdot \tau_A \otimes \tau_A \quad (45)$$

we obtain an expression which retains the interpretation of the tangential relative velocity in the case where perfect sliding occurs (i.e. when $\dot{\mathbf{g}}_A = 0$), but which contains the modification

necessary to make the velocity measure objective under all conditions of contact. This is readily seen by using direct calculation to exactly reexpress (45) as

$$\mathbf{v}_{T_A} = -\kappa_A \left[\sum_C \dot{n}_{AC}^{(2)} \Phi_C^{(2)} - \sum_B \dot{n}_{AB}^{(1)} \Phi_B^{(1)} \right] \cdot \boldsymbol{\tau}_A \otimes \boldsymbol{\tau}_A \quad (46)$$

where $\dot{n}_{AC}^{(2)}$ and $\dot{n}_{AB}^{(1)}$ are time derivatives of the mortar integrals (holding node A constant). Since these mortar integral time derivatives are the same in frame $*$ as they are in the original spatial frame, it is a straightforward matter to prove that \mathbf{v}_{T_A} satisfies (43) and is therefore frame indifferent.

Accordingly, a trial state-return map strategy is employed to determine the Coulomb frictional tractions in an algorithmic, time stepping procedure. As in Reference [7], we first compute a trial state, assuming no slip during the increment:

$$\lambda_{T_{A_{n+1}}}^{\text{trial}} = \lambda_{T_{A_n}} - \varepsilon_T \kappa_A \boldsymbol{\tau}_A \cdot \left[\sum_C \left(n_{AC_{n+1}}^{(2)} - n_{AC_n}^{(2)} \right) \Phi_C^{(2)} - \sum_B \left(n_{AB_{n+1}}^{(1)} - n_{AB_n}^{(1)} \right) \Phi_B^{(1)} \right] \quad (47)$$

and we define a trial value for the slip function via

$$\Phi_{n+1}^{\text{trial}} = \|\lambda_T^{\text{trial}}\| - \mu \|\lambda_N\| \quad (48)$$

Then the return map used to define the final frictional traction is given as:

$$\lambda_{T_{A_{n+1}}} = \begin{cases} \lambda_{T_{A_{n+1}}}^{\text{trial}} = \lambda_{T_{A_{n+1}}}^{\text{trial}} \boldsymbol{\tau}_A & \text{if } (\Phi_{n+1}^{\text{trial}}) \leq 0, \text{ stick} \\ \mu \|\lambda_{N_A}\| \boldsymbol{\tau}_A & \text{otherwise, slip} \end{cases} \quad (49)$$

In these expressions, the subscript $n+1$ means a state associated with the current iteration of the $n+1$ st load (or time) step, and n is to be associated with the n th converged load step.

5. NUMERICAL INTEGRATION OF THE MORTAR INTEGRAL

Both of integrals (31) and (32) are performed on the slave surface; however, the expression in (32) has an integrand with terms defined on two different surfaces. Thus, the mortar integral $n_{AC}^{(2)}$ must be carefully subdivided such that each subdomain of integration (termed a *mortar segment* in this work) contains smooth contributions from both $\gamma^{(1)h}$ and $\gamma^{(2)h}$. In the formulation proposed in this paper, each mortar segment contains contributions from only one element from each contacting surface. The notation of the mortar segment is directly analogous to the contact segment proposed by Simo *et al.* [19]. Here, a new method is proposed to define the mortar segment and it is based on the definition of the continuous normal fields on the slave surface ($\gamma^{(1)h}$).

5.1. Definition of nodal normal and tangential directions, \mathbf{n}_A and $\boldsymbol{\tau}_A$

As mentioned previously, the discretization process induces a faceted contact geometry, which gives sudden changes of surface normal and tangent vectors at contact nodes (see Figure 2). The discontinuity of these basis vectors can adversely affect the robustness of the algorithm,

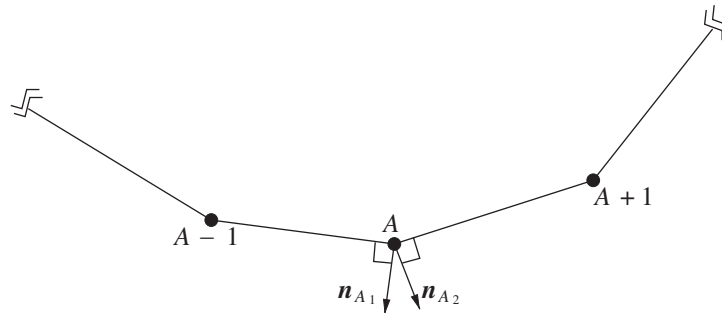


Figure 2. Discontinuous normal vectors on a discretized contact surface.

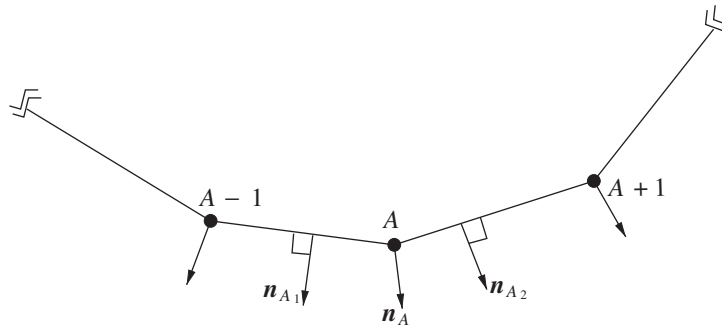


Figure 3. Notation for definition of continuous normal fields on a discretized contact surface.

especially where the searching for mortar segments is concerned. Furthermore, in definition of the nodal gap in (36), we need some notion of unique normal vector to resolve the normal and tangential directions associated with the interface response. Here, we propose a simple averaging method to determine these nodal basis vectors, which are used both in our mortar segmentation algorithm and to resolve our contact constraints.

In this paper, a continuous normal field is defined on the slave surface, based on a uniquely defined normal vector at each slave node. As illustrated in Figure 3, a unique normal vector is defined at node A , which is the weighted average of the outward normal vectors on the two adjacent elements which share the node A . The definition of the normal vector \mathbf{n}_A at node A is

$$\mathbf{n}_A = \frac{\hat{\mathbf{n}}_A}{\|\hat{\mathbf{n}}_A\|} \quad (50)$$

where

$$\hat{\mathbf{n}}_A = l_2 \mathbf{n}_{A1} + l_1 \mathbf{n}_{A2} \quad (51)$$

with \mathbf{n}_{A1} and \mathbf{n}_{A2} being the normal vectors defined on the two elements intersecting at node A . The quantities l_1 and l_2 are the lengths of the two adjacent edges.

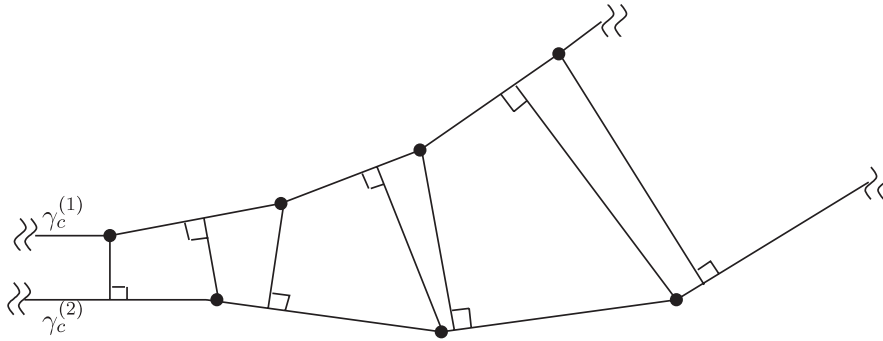


Figure 4. Traditional technique for mortar segment searching, depending on closest point projection.

With this definition of normal vectors, the unit tangential vector is defined as

$$\boldsymbol{\tau}_A = \mathbf{e}_3 \times \mathbf{n}_A \quad (52)$$

Furthermore, with these definitions in hand, we can define continuous normal fields on the entire surface by using linear interpolation. The continuous normal vector at position ξ of a slave element is represented as

$$\mathbf{n}_e(\xi) = \sum_A N_A^{(1)}(\xi) \mathbf{n}_A \quad (53)$$

where \mathbf{n}_A , defined in (50), is the normal vector at node A , and $N_A^{(1)}$ is the shape function associated with node A (restricted to the element boundary, as before). The continuous normal vector will be seen to be useful in searching for mortar segments.

5.2. Searching for mortar segments

5.2.1. Traditional method based on closest point projection. There are at least two different ways to construct mortar segments. The first method, employed in Reference [14], is similar to the construction of contact segments given in Reference [6]. In Reference [14], the outer nodes of each element comprising each of the two contacting surfaces are projected onto the surfaces opposing them, as illustrated in Figure 4. These nodes and their projections then define the extremities of the contact segments. Although techniques exist to make this algorithm robust, there are some obvious cases in which extra heuristics are required to make the procedure perform adequately. For example, the discontinuity at each corner can cause troubles for the projections (as would be true also for a node-to-surface contact treatment). As shown in Figure 5, when the closest point projection of the slave point onto the master element is a corner (because of the discontinuity), the direction associated with the projection is no longer coincident with the master side normals, and the linearization of this operator varies discontinuously as the slave node moves through the region of the corner. A second problem is also shown in Figure 5, and occurs when the normals associated with adjacent projections actually cross each other; if one uses this searching procedure, one must actually tolerance out such crossings when defining the segments.

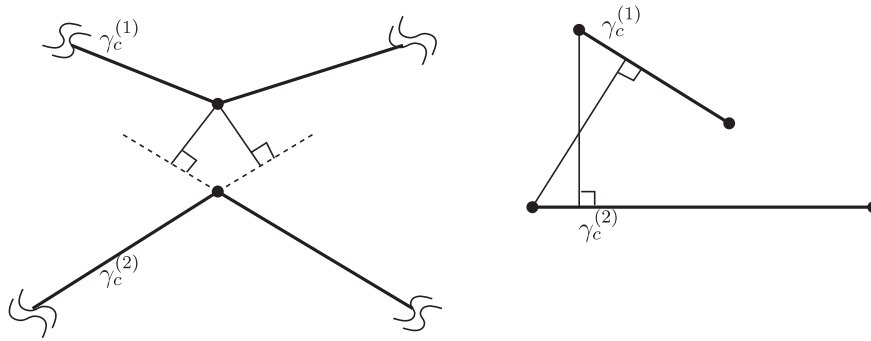


Figure 5. Potential non-robustnesses in traditional mortar segment searching algorithm.

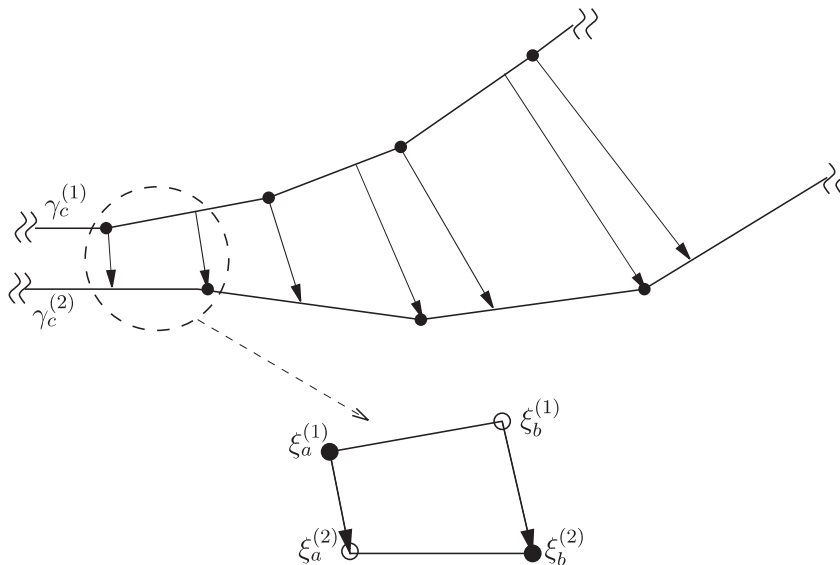


Figure 6. The new mortar segmentation method. A typical segment is shown.

5.2.2. A new two dimensional segmentation method. In this paper, a new method is employed to construct mortar segments, which is consistent with the definition of continuous normal fields in the last section. Figure 6 illustrates a typical result obtained from this algorithm. In this strategy, a continuous normal field on the slave surface is used to accomplish *both* sets of projections (i.e. slave to master and master to slave). The projection of a slave node onto the master surface is quite straightforward, and only requires finding the intersection of the master surface with a line emanating from the slave node along \mathbf{n}_A . Projection of a master node onto the slave surface involves finding that point on the slave surface where the continuously defined normal points toward the master node; this calculation necessitates solution of a quadratic equation for linear elements (cubic for quadratic elements).

Specifically, if we wish to find the projection of a slave node $\boldsymbol{\phi}_s^{(1)}$, having normal vector $\mathbf{n}_s^{(1)}$, onto a master element with nodes $\boldsymbol{\phi}_1^{(2)}$ and $\boldsymbol{\phi}_2^{(2)}$, we can accomplish this via solution of

$$\left[N_1(\xi^{(2)})\boldsymbol{\phi}_1^{(2)} + N_2(\xi^{(2)})\boldsymbol{\phi}_2^{(2)} - \boldsymbol{\phi}_s^{(1)} \right] \times \mathbf{n}_s^{(1)} = \mathbf{0} \quad (54)$$

where $\xi^{(2)}$ is the parent co-ordinate of the projection of the slave node onto the master element. In (54), which is a linear equation having only one solution, N_1 and N_2 are two shape functions associated with the two master nodes. On the other hand, the equation to find the projection of a master node $\boldsymbol{\phi}_m^{(2)}$ onto a slave element with nodes $\boldsymbol{\phi}_1^{(1)}$ and $\boldsymbol{\phi}_2^{(1)}$ is

$$\left[N_1(\xi^{(1)})\boldsymbol{\phi}_1^{(1)} + N_2(\xi^{(1)})\boldsymbol{\phi}_2^{(1)} - \boldsymbol{\phi}_m^{(2)} \right] \times \left[N_1(\xi^{(1)})\mathbf{n}_1 + N_2(\xi^{(1)})\mathbf{n}_2 \right] = \mathbf{0} \quad (55)$$

where $\xi^{(1)}$ denotes the projection of the master node onto the slave element. In (55), which is a quadratic equation for a linear element, N_1 and N_2 are the shape functions associated with the two slave nodes, and \mathbf{n}_1 and \mathbf{n}_2 are the two normal vectors defined on the two slave nodes.

With these ideas, the procedure to find the node-segment pairs over which these calculations are performed can be outlined as follows:

1. As part of the initialization procedure, a global searching procedure is performed to find the closest master element to each slave node and the closest slave element to each master node. To find the closest master element to a slave node, we find the intersection of all master elements with the line pointing from the slave node along the direction of the normal vector at the slave node. The master element having the intersection closest to the slave node is the one selected.

To find the closest slave element to a master node, we first find the closest slave node to the master node. There will be two slave elements connected with this node, and a slave normal as well. The closest slave element is then determined by the side of the normal on which the master node falls.

2. In every subsequent equilibrium iteration, we perform a local search only to find the closest elements to each slave and master node. The local search is only performed in the neighborhood of the closest element in the last iteration. Of course, this local search must be replaced by a more sophisticated algorithm in the instance of self-contact (see Reference [4]).

In each iteration, we loop over all pairs of slave and master elements to find all possible mortar segments. Those elements which are far from each other are sorted out in this procedure, so that the mortar projection is only performed over segments defined by valid projections and whose opposing surfaces are within some user-specified tolerance of each other.

5.3. Adding the segment contributions

The integrations indicated in (31) and (32) are performed by subdivision of the elements into mortar segments. The integrals are then computed by summing over all such segments on the

entire surface, via

$$n_{AB}^{(1)} = \sum_{\text{seg}} n_{AB}^{(1)\text{seg}}$$

$$n_{AB}^{(1)\text{seg}} = \int_{\gamma_c^{\text{seg}}} N_A^{(1)}(\xi^{(1)}(\mathbf{X})) N_B^{(1)}(\xi^{(1)}(\mathbf{X})) d\gamma \quad (56)$$

$$n_{AC}^{(2)} = \sum_{\text{seg}} n_{AC}^{(2)\text{seg}}$$

$$n_{AC}^{(2)\text{seg}} = \int_{\gamma_c^{\text{seg}}} N_A^{(1)}(\xi^{(1)}(\mathbf{X})) N_C^{(2)}(\xi^{(2)}(\bar{\mathbf{Y}}(\mathbf{X}))) d\gamma \quad (57)$$

where seg denotes the mortar segments and γ_c^{seg} denotes a segment surface. A typical mortar segment is shown in Figure 6.

5.4. Mapping from segment co-ordinates to element co-ordinates

To perform numerical quadrature of (56) and (57), a parameterization η of a typical mortar segment is introduced. This variable ranges between -1 and 1 over each mortar segment.

Defining the element co-ordinates of the four ends of a mortar segment (two slave and two master) as $\xi_a^{(1)}$, $\xi_b^{(1)}$, $\xi_a^{(2)}$ and $\xi_b^{(2)}$ (see Figure 6), a mapping from the η to $\xi^{(i)}$, $i = 1, 2$, is given by

$$\xi^{(i)} = \frac{1}{2}(1 - \eta)\xi_a^{(i)} + \frac{1}{2}(1 + \eta)\xi_b^{(i)} \quad (58)$$

With these definitions and notations, the segment contributions in (56) and (57) are rewritten as integrals on η as

$$n_{AB}^{(1)\text{seg}} = \int_{-1}^1 N_A^{(1)}(\xi^{(1)}(\eta)) N_B^{(1)}(\xi^{(1)}(\eta)) \left\| \frac{\partial \Phi_e^{(1)h}}{\partial \xi^{(1)}} \right\| \frac{\partial \xi^{(1)}}{\partial \eta} d\eta \quad (59)$$

$$n_{AC}^{(2)\text{seg}} = \int_{-1}^1 N_A^{(1)}(\xi^{(1)}(\eta)) N_C^{(2)}(\xi^{(2)}(\eta)) \left\| \frac{\partial \Phi_e^{(1)h}}{\partial \xi^{(1)}} \right\| \frac{\partial \xi^{(1)}}{\partial \eta} d\eta \quad (60)$$

By employing a numerical quadrature rule, we may write the approximation for $n_{AB}^{(1)\text{seg}}$ and $n_{AC}^{(2)\text{seg}}$ via

$$n_{AB}^{(1)\text{seg}} \approx \sum_{g=1}^{n_g} w_g N_A^{(1)}(\xi^{(1)}(\eta_g)) N_B^{(1)}(\xi^{(1)}(\eta_g)) J_{\text{seg}} \quad (61)$$

$$n_{AC}^{(2)\text{seg}} \approx \sum_{g=1}^{n_g} w_g N_A^{(1)}(\xi^{(1)}(\eta_g)) N_C^{(2)}(\xi^{(2)}(\eta_g)) J_{\text{seg}} \quad (62)$$

where η_g are the segment co-ordinates of quadrature points, n_g is the number of segment quadrature points, w_g is the weight of the quadrature point, and J_{seg} is the jacobian at the

quadrature point, given as

$$J_{\text{seg}} = \left\| \frac{\partial \Phi_e^{(1)h}}{\partial \eta} \right\| = \left\| \frac{\partial \Phi_e^{(1)h}}{\partial \xi^{(1)}} \right\| \left| \frac{\partial \xi^{(1)}}{\partial \eta} \right| \quad (63)$$

In the investigations reported in this paper, five point Gauss rules are used to evaluate the segment mortar integrals in (61) and (62).

6. LINEAR AND ANGULAR MOMENTUM CONSERVATION

As discussed more extensively in Reference [18], the linear and angular momentum conservation properties are intricate for mortar methods. Here we summarize briefly the results for the proposed two dimensional formulation.

6.1. Linear momentum conservation

The algorithm proposed exactly conserves linear momentum; i.e. it ensures that the total forces on slave and master surfaces are in equilibrium. When we formulate contact virtual work, we suppose that:

$$\lambda^{(1)} d\gamma^{(1)} = \lambda^{(2)} d\gamma^{(2)} \quad (64)$$

So, on a contact segment, we have

$$\begin{aligned} \mathbf{f}_{\text{seg}}^{(1)} - \mathbf{f}_{\text{seg}}^{(2)} &= \int_{\gamma_{\text{seg}}^{(1)}} \lambda^{(1)} d\gamma^{(1)} - \int_{\gamma^{(2)}} \lambda^{(2)} d\gamma^{(2)} \\ &= \int_{\gamma_{\text{seg}}^{(1)}} \left(\sum_A \lambda_A N_A - \sum_A \lambda_A N_A \right) d\gamma^{(1)} = \mathbf{0} \end{aligned} \quad (65)$$

so that linear momentum is conserved.

6.2. Angular momentum conservation

Angular momentum may not be conserved. The net value of moment on slave and master surfaces can be computed as

$$\begin{aligned} \mathbf{M} &= \int_{\gamma_c^{(1)}} \lambda \times (\boldsymbol{\phi}^{(1)} - \boldsymbol{\phi}^{(2)}) d\gamma^{(1)} \\ &= \sum_{\text{seg}} \int_{\gamma_{\text{seg}}^{(1)}} \sum_A \lambda_A N_A \times \left(\sum_B N_B \boldsymbol{\phi}_B^{(1)} - \sum_C N_C \boldsymbol{\phi}_C^{(2)} \right) d\gamma^{(1)} \\ &= \sum_A \lambda_A \times \left[\sum_B n_{AB}^{(1)} \boldsymbol{\phi}_B^{(1)} - \sum_C n_{AC}^{(2)} \boldsymbol{\phi}_C^{(2)} \right] \end{aligned} \quad (66)$$

This is zero only when λ_A is in the same direction as $\left[\sum_B n_{AB}^{(1)} \boldsymbol{\phi}_B^{(1)} - \sum_C n_{AC}^{(2)} \boldsymbol{\phi}_C^{(2)} \right]$ or when $\left[\sum_B n_{AB}^{(1)} \boldsymbol{\phi}_B^{(1)} - \sum_C n_{AC}^{(2)} \boldsymbol{\phi}_C^{(2)} \right] = \mathbf{0}$. For frictional contact problems, $\left[\sum_B n_{AB}^{(1)} \boldsymbol{\phi}_B^{(1)} - \sum_C n_{AC}^{(2)} \boldsymbol{\phi}_C^{(2)} \right]$

will not in general be parallel to λ_A . On the other hand, $\left[\sum_B n_{AB}^{(1)} \Phi_B^{(1)} - \sum_C n_{AC}^{(2)} \Phi_C^{(2)}\right]$ is also not in general zero, particularly since we are employing penalty methods. In most cases we can expect that $\left[\sum_B n_{AB}^{(1)} \Phi_B^{(1)} - \sum_C n_{AC}^{(2)} \Phi_C^{(2)}\right]$ will be near zero; in cases where it is not, or where exact angular momentum conservation is important, intricate (but expensive) modifications to the algorithm are possible.

7. LINEARIZATION OF CONTACT VIRTUAL WORK

In applying a Newton–Raphson method to the discretized version of the contact problem (6), we employ consistent algorithmic linearization to iteratively solve the non-linear problem through a series of linear ones. Since the details involved in this linearization are quite involved, the discussion of this topic is deferred here to Appendix A. That appendix presents highlights of the procedure necessary to calculate the mortar contact stiffness, beginning with the approximation summarized in (30).

8. NUMERICAL EXAMPLES

In this section, the robustness and accuracy of the mortar element method for large deformation contact problems is demonstrated by several numerical examples.

8.1. A contact patch test

If a contact surface between two bodies is subjected to a spatially constant stress field, it should be able to exactly transmit this stress field from one body to another. If it can do so for arbitrary non-conforming contact surfaces, the contact formulation passes the patch test [7]. Here we use the test method originally designed by Simo *et al.* [19] as a benchmark problem for the finite element treatment of contact problems.

The configuration of the problem is shown in Figure 7, and corresponds to an elastic punch being pressed onto an elastic foundation. To make the problem more generally representative, the punch is offset from the centre of the foundation. A uniform pressure of $p = 100.0$ is applied to the upper surface of both the punch and the foundation. The punch and the foundation are taken as linear isotropic elastic media with the same material properties, and plane stress conditions are assumed.

We assume that $E = 1000.0$ and $\nu = 0.4$; the finite element discretization of the problem is shown in Figure 8. Figure 9 shows the deformed and undeformed configurations. The dotted line is the deformed configuration. One may note also the non-conforming and non-uniform meshes along the contact interface. The results shown correspond to a penalty of 10^7 ; the patch test is passed to machine precision.

8.2. Hertzian contact

A cylinder on cylinder Hertzian contact problem is presented next, to investigate the accuracy of the proposed formulation. Because the analytical solution is for infinitesimal deformation, we need to apply a very small load for this problem. As a result, the contact region is relatively small. The cylinders are modelled as isotropic linear elastic materials ($E = 200.0$, $\nu = 0.3$),

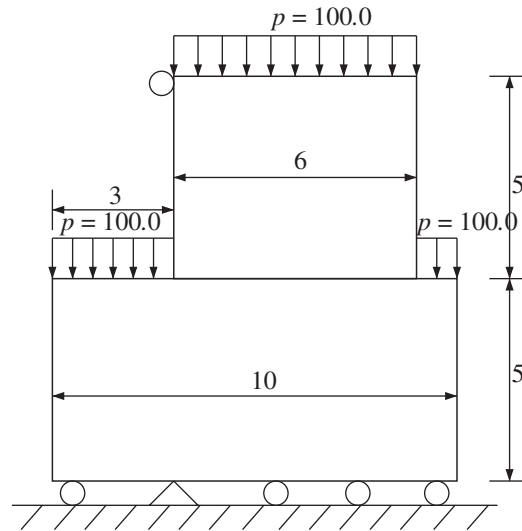


Figure 7. Contact patch test problem definition.

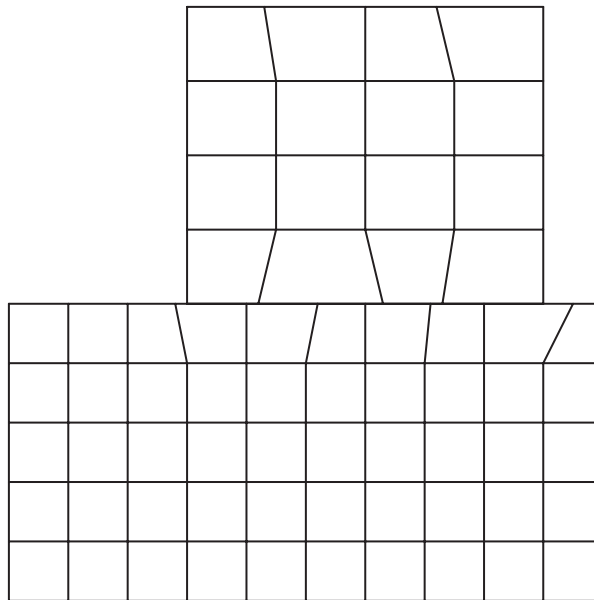


Figure 8. Contact patch test mesh.

and the penalty parameters are $\varepsilon_N = 5.0 \times 10^5$, $\varepsilon_T = 5.0 \times 10^5$. The coefficient of friction is 0.2 (Figure 10).

Two parallel half cylinders are pressed by a distributed pressure p , which will induce a normal contact force P at the point of contact. Subsequently, a second distributed load q is

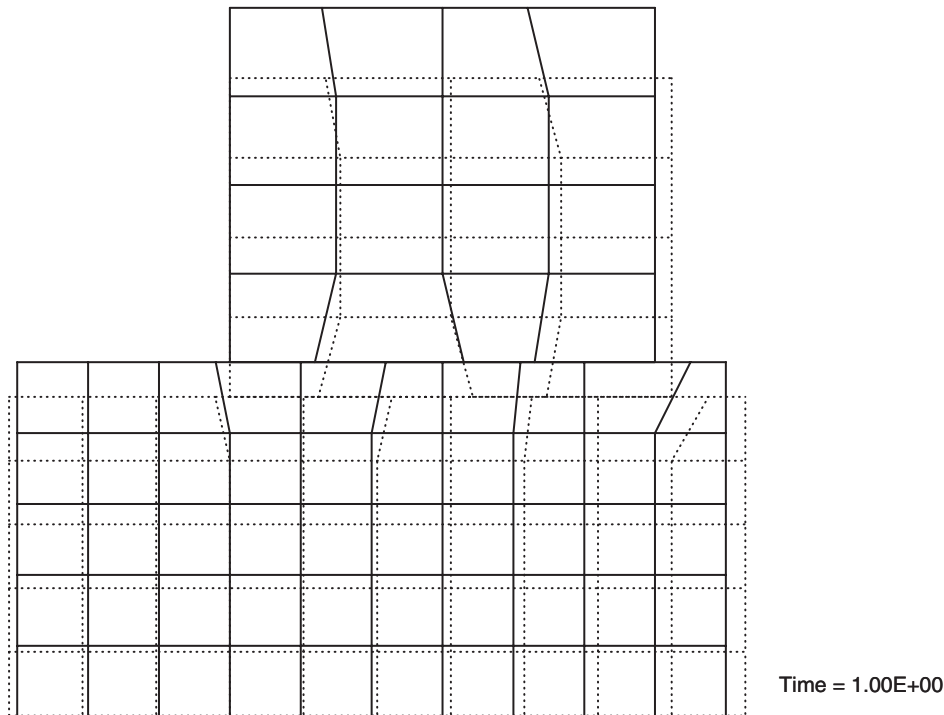


Figure 9. Deformed and undeformed meshes for the contact patch test.

applied in the tangential direction of the plane. This load induces a frictional contact force Q at the contact point. The load histories for p and q are given in Figure 11 where $p_{\max} = 0.625$ and $q_{\max} = 0.05851$ with respect to $P_{\max} = 10$ and $Q_{\max} = 0.93622$, where P_{\max} and Q_{\max} are the total reaction forces over the slave surface, in the vertical and horizontal directions.

The finite element meshes are shown in Figure 12; while the comparison of the numerical result and the analytical solution [20] for the surface tractions is given in Figure 13. There are some small differences between the solutions because we use a large deformation formulation; furthermore, some spatial oscillations in the numerical solution for the frictional traction are present, seemingly due to the nonsmoothness of the frictional traction field at the stick slip boundary. Notably, these oscillations disappear for fine meshes (see Figure 14).

8.3. Hyperelastic frictional beam contact problem

This problem is intended to test the robustness of the formulation in the context of a truly large deformation frictional contact problem. A neo-Hookean hyperelastic constitutive model is considered for this problem, with material parameters $K = G = 1000.0$ for the curved and $K = 3000.0$, $G = 1000.0$ for the straight beam. As shown in Figure 15, a curved beam is fixed on one end in the y direction and subjected to a vertical displacement $d_y = 1.2t$ at the other end. Simultaneously, a horizontal displacement $d_x = 2.0t$ is applied at both beam ends. In this problem, we set $t_{\max} = 8$, so that $d_{y_{\max}} = 9.6$ and $d_{x_{\max}} = 16$. The straight beam in the figure is simply supported.

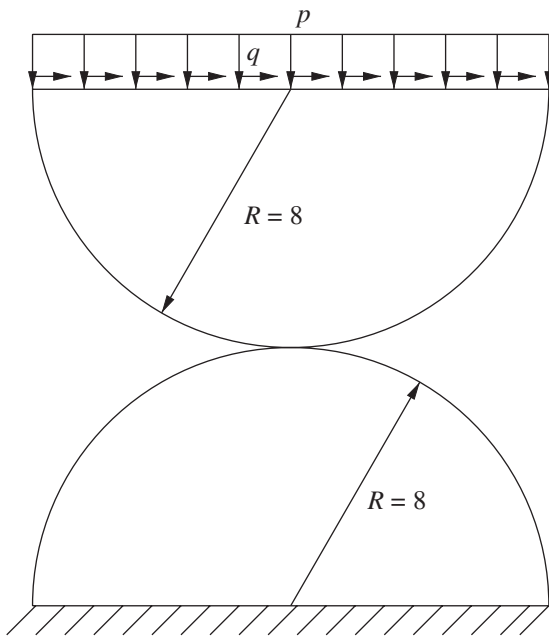


Figure 10. The schematic of cylinder on cylinder Hertzian contact problem.

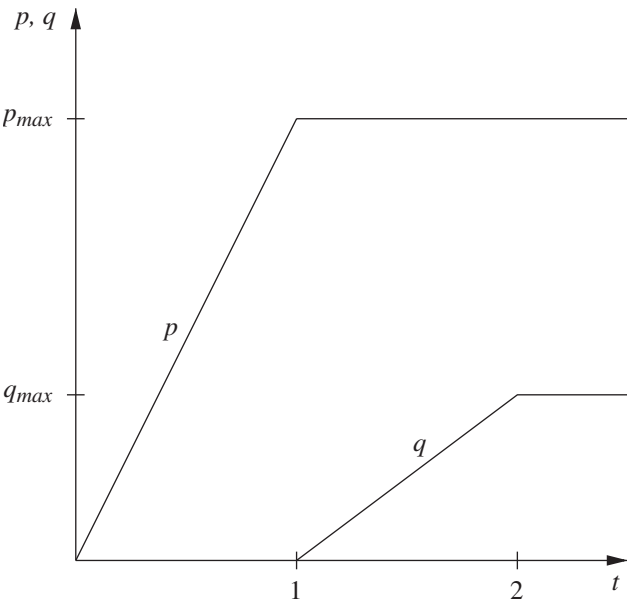


Figure 11. Load histories of the cylinder on cylinder Hertzian contact problem.

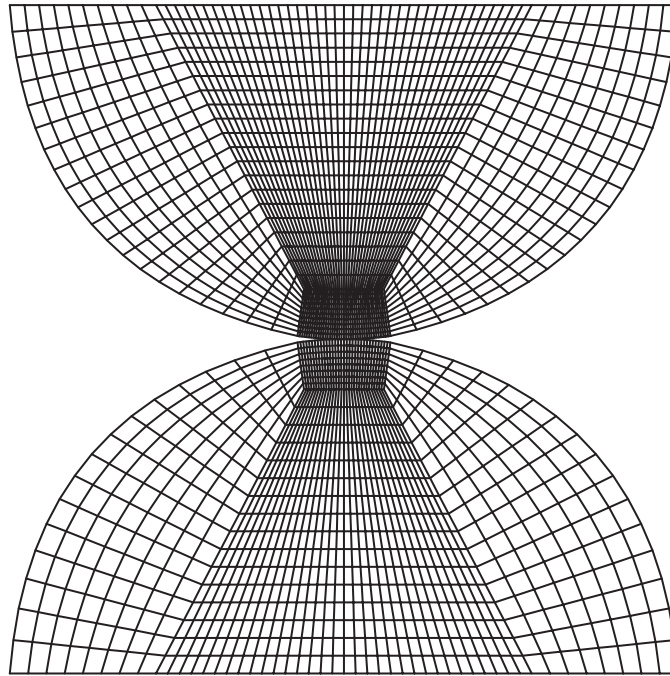


Figure 12. The mesh for the Hertzian contact problem.

At the beginning, the two beams are in grazing contact. With the deformation of the curved beam, it applies contact pressure and frictional traction to the straight beam. We consider Coulomb friction in this problem and the coefficient of friction is $\mu = 0.5$.

Figure 16 depicts the discretization of the problem. The penalty parameters are $\varepsilon_N = \varepsilon_T = 5.0 \times 10^3$. The simulation was run over the time interval $[0, 8.0]$ with time increments $\Delta t = 0.025$.

The evolution of the deformation of the two beams is shown in Figure 17, depicting the deformed mesh at the times $t = 2.0, 4.0, 6.0$ and 8.0 . The large deformation and large sliding of the problem are apparent in this figure. The reaction forces in the y direction at the left support of the straight beam are shown in Figures 18 and 19. Results are shown both for the mortar method proposed in this paper, as well as for the traditional node to surface contact formulation. Results are also shown with both choices of master/slave pairings, for both formulations. Although at first glance the results are relatively insensitive to the method chosen (see Figure 18), the zoom shown in Figure 19 reveals the oscillations inherent to a node to surface method for both choices of master–slave pairings, and significant reduction of these oscillations for the mortar method. Also, the amount of variation in the results with the two choices of master–slave pairings is significantly smaller for the mortar method than it is for the traditional method.

8.4. A finite deformation frictional plastic contact problem

The next example is another with large deformations and large sliding. It demonstrates the applicability of proposed method to problems involving material as well as geometric

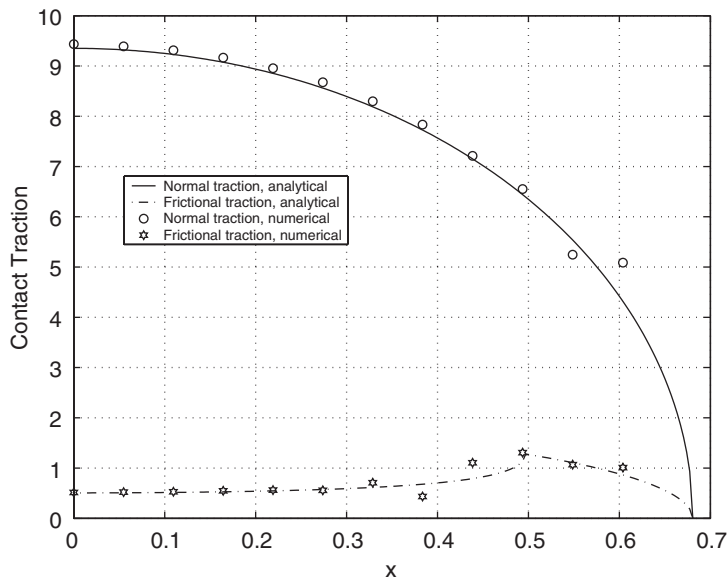


Figure 13. Computed nodal contact traction for frictional cylinder on cylinder contact problem; coarse mesh.

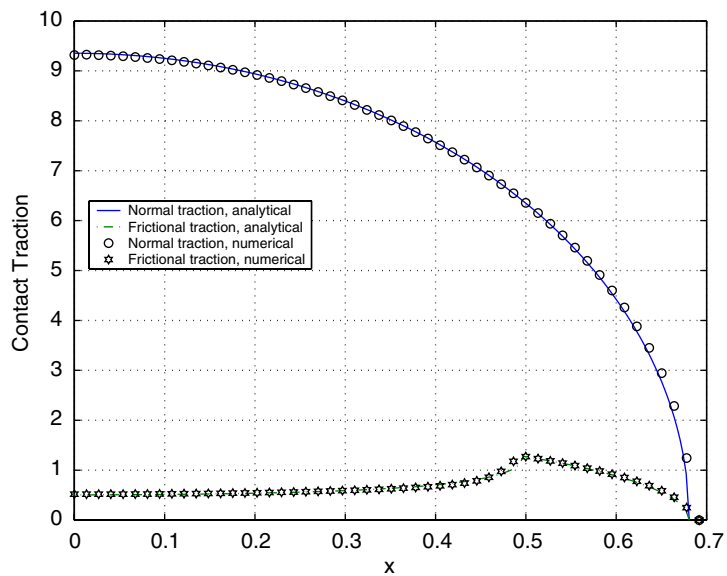


Figure 14. Computed nodal contact traction for frictional cylinder on cylinder contact problem; finer mesh.

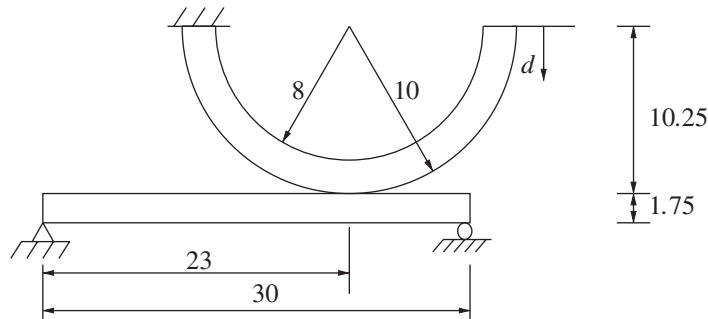


Figure 15. Schematic of the hyperelastic beam contact problem.

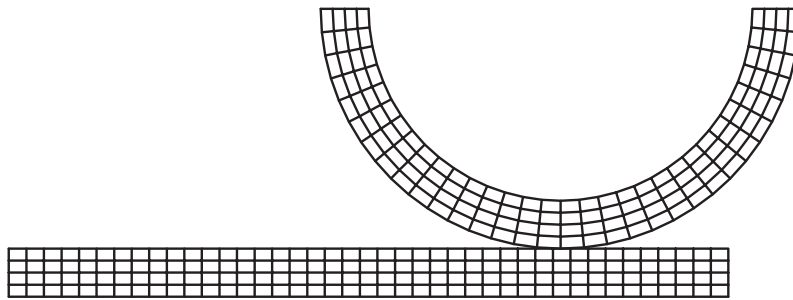


Figure 16. The discretization of the hyperelastic beam contact problem.

non-linearities. We consider two contacting curved beams as shown in Figure 20. One beam is fixed and another is given a horizontal displacement $d = t$ with $d_{\max} = 31.2$, i.e. $t_{\max} = 31.2$. Both beams are modelled using a finite deformation isotropic hardening elasto-plastic material, with material properties taken as $K = 0.6384$ GPa, $G = 0.2612$ GPa, $\sigma_y = 31$ MPa and $H = 0.2612$ GPa, where K and G are the bulk and shear moduli, respectively, σ_y is the yield stress and H is the plastic modulus.

The two curved beams were discretized as shown in Figure 21. The penalty parameters are $\varepsilon_T = \varepsilon_N = 3.5 \times 10^8$. The coefficient of friction is $\mu = 0.3$. Over the time interval $[0, 31.0]$, the time increments were taken as $\Delta t = 0.5$. There is one time step from 31.0 to 31.2.

The evolution of deformation and plastic regions is depicted in Figure 22, which shows the contour of the effective plastic strain. As expected, the plastic region originates near the contact area, and grows, ultimately producing some permanent deformation which is apparent in the figure. The sequence of convergence of the energy norm is shown in Table I for representative time steps from this simulation. From the table, we can see this method converges quite quickly even for time steps including large deformation and sliding. For a node-to-segment formulation, the computation fails at some early time step even with much smaller time steps. Table II presents the comparison of CPU time for the two approaches with $t = 0.0$ to 22.5. It gives the comparisons with same time steps where approaches converge and larger time steps

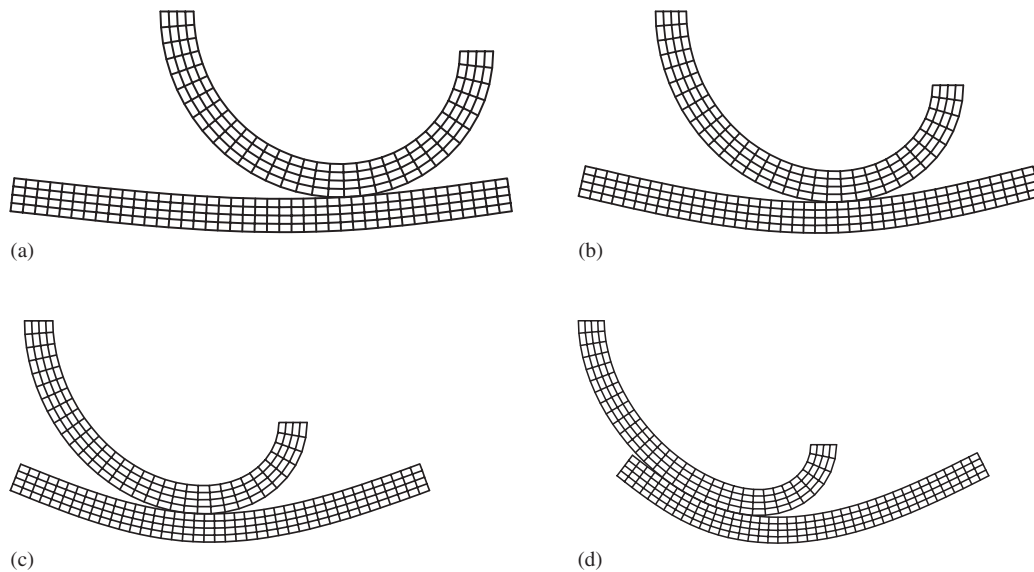


Figure 17. Deformed configurations for hyperelastic beam contact problem:
(a) $t = 2.0$; (b) $t = 4.0$; (c) $t = 6.0$; and (d) $t = 8.0$.

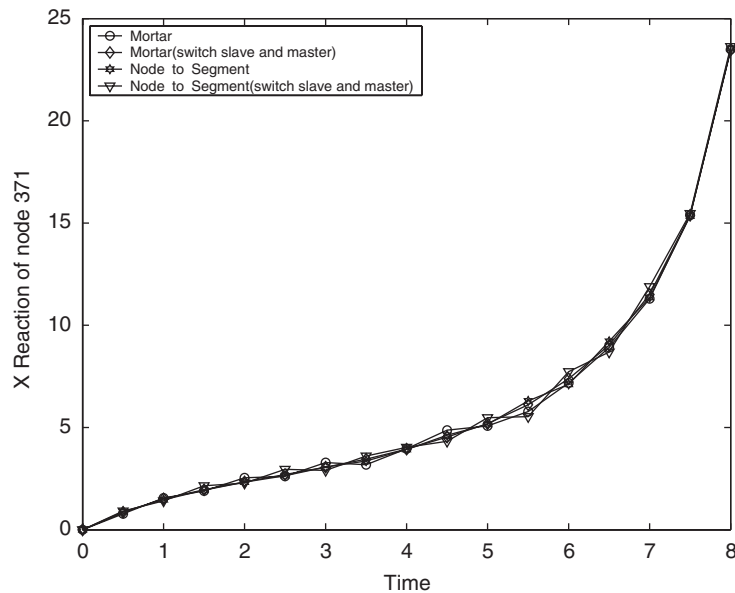


Figure 18. Reaction force at the left support of the straight beam; hyperelastic beam problem.

for the mortar method. From Table II, we can see the node-to-surface method takes more time because it takes more iterations to converge. In each iteration, it is a little cheaper than the mortar method. In an overall sense, the mortar method is still much cheaper.

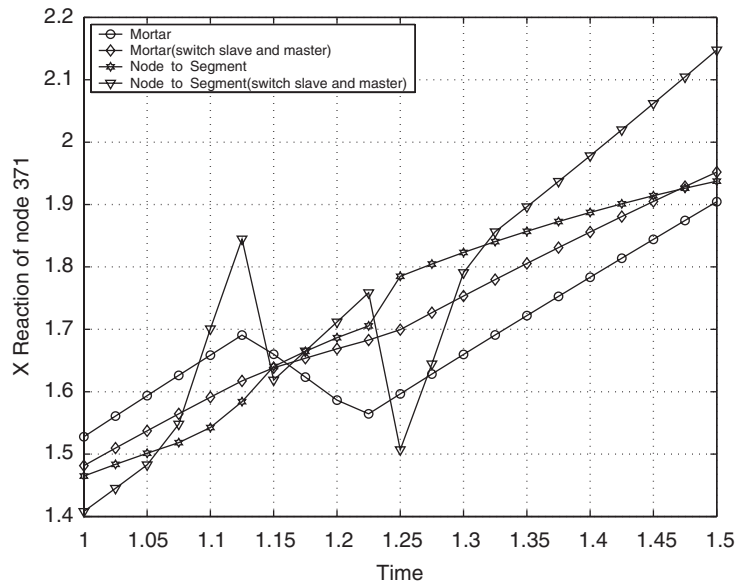


Figure 19. Reaction force at the left support of the straight beam; hyperelastic beam problem. Zoom of region for $t \in [1, 1.5]$.

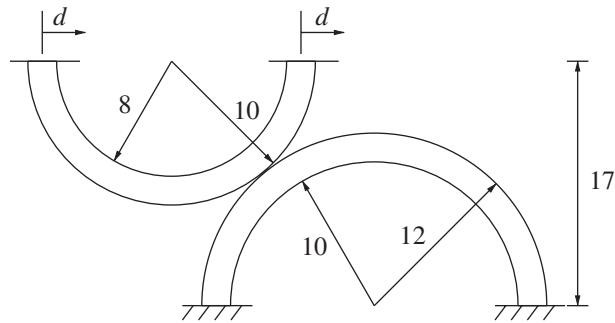


Figure 20. Schematic of the large deformation plastic contact problem.

To further illustrate the performance of this method, a larger time increment $\Delta t = 2.5$ was applied at $t = 5.0$ and it still can get convergence. This is shown in Figure 23 with the deformed mesh at $t = 5.0$ and 7.5 (bold). The convergence sequence of this time step is shown in Table III. The struggle from 2nd to 7th iterations is because the time step is large and line search ultimately facilitates convergence. The largest time step that can be used in this problem with the node-to-segment formulation is only $t = 0.56$.

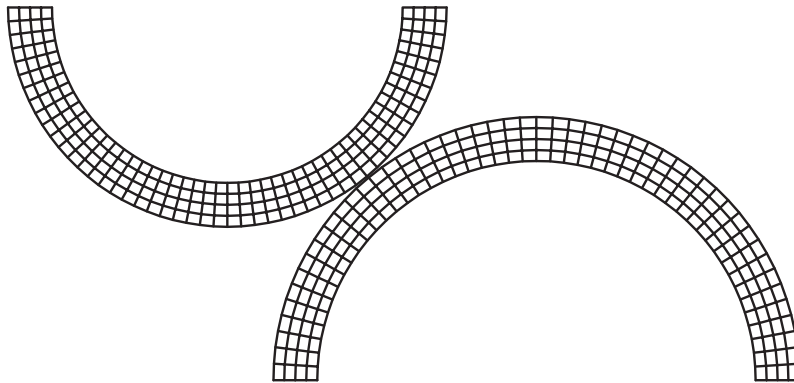
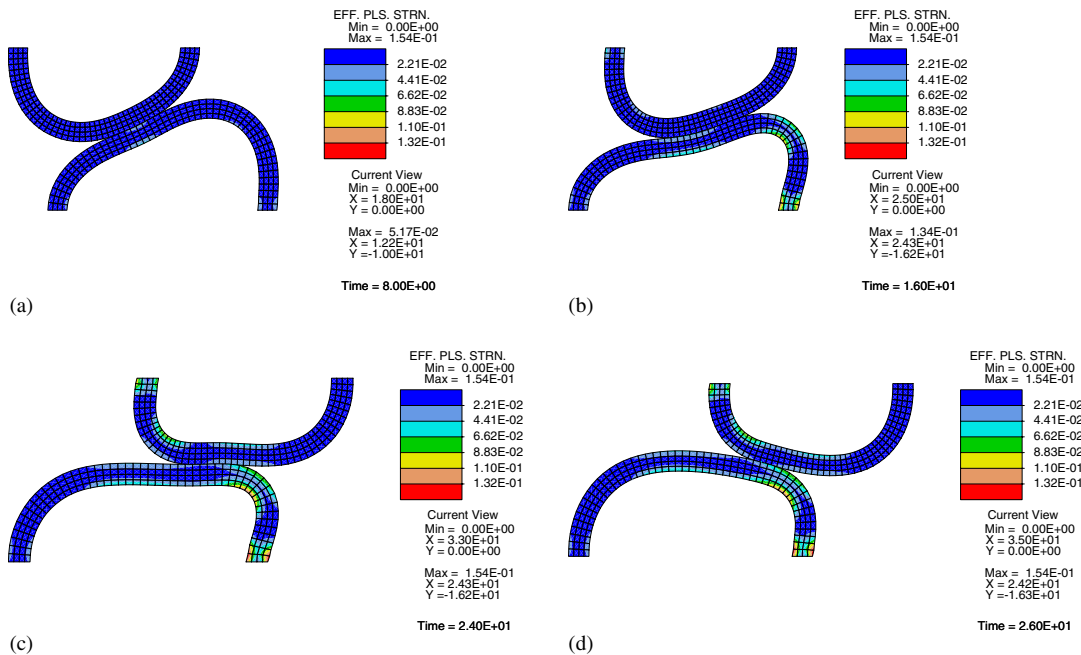


Figure 21. Discretization of the large deformation plastic contact problem.

Figure 22. Deformed configurations with effective plastic strain contours for large deformation plastic contact problem: (a) $t = 8$; (b) $t = 16$; (c) $t = 24$; and (d) $t = 26$.

8.5. An ironing problem

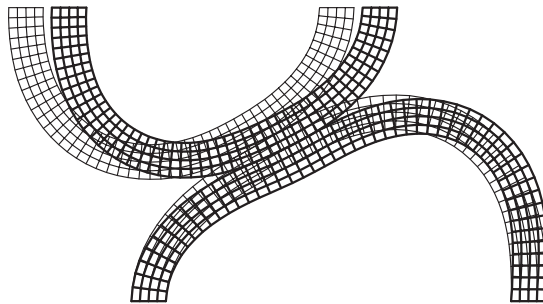
In this problem, a block is pressed into the slab and then slid over the surface. The material for both the block and the slab are assumed to be Neo-Hookean hyperelastic. The bulk and shear modulus of the slab are $K = 63.84 \times 10^7$ and $G = 26.12 \times 10^7$. The block is 10 times

Table I. Convergence behaviour, in terms of energy norm, for some representative time steps; large deformation plastic contact problem.

Iteration No.	8	16	24	32	40	52
1	9.85E-03	8.77E-03	8.40E-03	2.75E-03	5.31E-03	2.45E-03
2	1.42E-04	4.02E-04	1.03E-03	4.51E-03	6.37E-04	5.21E-04
3	6.04E-08	8.87E-07	7.46E-04	1.33E-03	1.63E-05	2.90E-06
4	3.60E-14	1.10E-10	1.90E-05	2.07E-03	3.33E-08	1.00E-09
5	7.94E-26	1.38E-19	2.83E-08	8.41E-06	9.78E-12	7.31E-17
6		1.24E-25	3.10E-15	7.58E-09	7.49E-19	1.99E-22
7			7.45E-25	2.92E-15	8.05E-24	
8				7.43E-20		
9				2.94E-24		

Table II. Comparison of the CPU time (in seconds) expended for the large deformation plastic contact problem for $t \in [0, 22.5]$: node to surface and mortar approaches.

Method	Total	Ave. per time step	Ave. per iter.
Node-to-Surface, $\Delta t = 0.5$	86.11	0.926	0.0462
Mortar, $\Delta t = 0.5$	60.06	0.652	0.0691
Mortar, $\Delta t = 2.5$	34.95	0.777	0.0789

Figure 23. The deformation for one large time step, $\Delta t = 2.5$, $t = 5.0$; large deformation plastic contact problem.

stiffer than the slab, so the bulk and shear modulus are $K = 63.84 \times 10^8$ and $G = 26.12 \times 10^8$, respectively. The geometric properties are shown in Figure 24. The bottom surface of the slab is fixed. The block travels $p = 1.8$ in the vertical direction from time 0 to 1 and then $q = 10$ in the horizontal direction from time 1 to 2. The finite element meshes are shown in Figure 25. The deformation at $t = 1.0$, 1.5 and 2.0 are shown in Figures 26, 27 and 28 respectively. Coulomb friction is considered in this problem, with the coefficient of friction being $\mu = 0.3$.

Table III. Energy norm for the large time step depicted in Figure 23.

Iteration no.	Energy norm
1	1.32E-02
2	8.12E-03
3	1.93E-03
4	6.42E-04
5	8.48E-04
6	2.37E-05
7	1.05E-07
8	8.43E-13
9	4.78E-19
10	4.19E-24

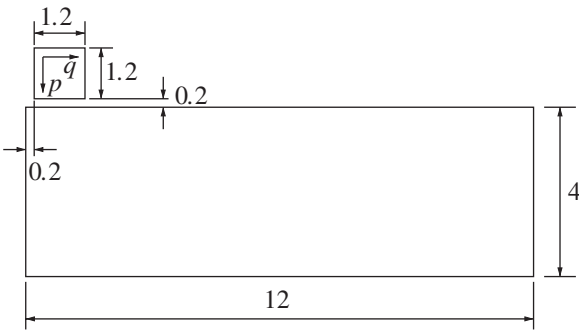


Figure 24. The initial configuration of the ironing problem.

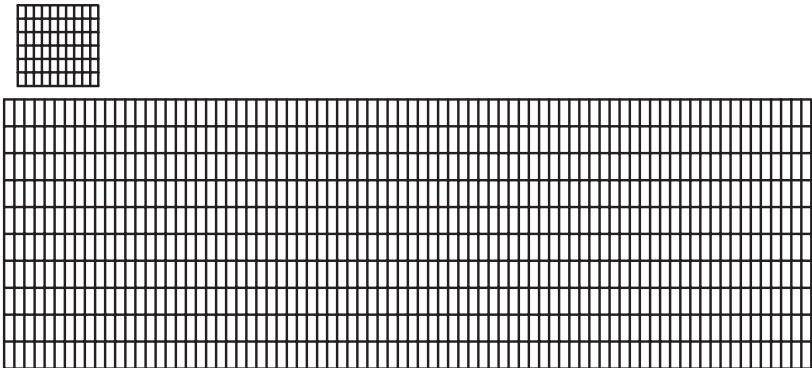


Figure 25. The finite element meshes of the ironing problem.

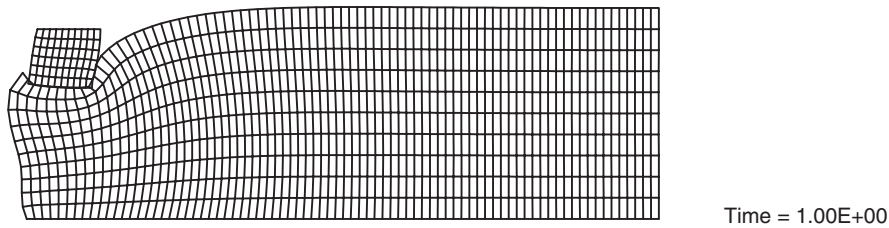


Figure 26. The deformation of the ironing problem at $t = 1.0$.

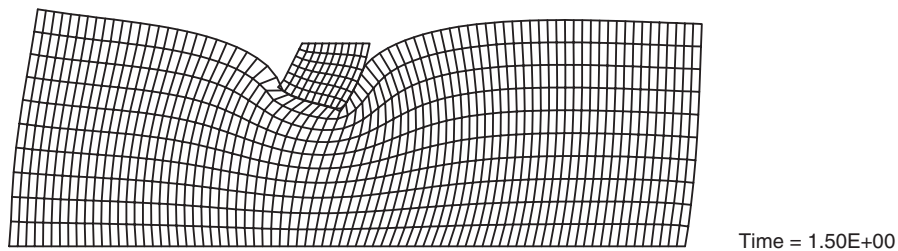


Figure 27. The deformation of the ironing problem at $t = 1.5$.

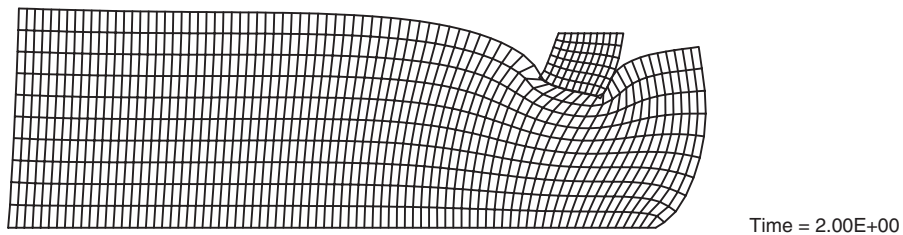


Figure 28. The deformation of the ironing problem at $t = 2.0$.

In this problem, the deformation of the slab is sufficient so that contact of the side surfaces of the block with the slab have to be considered; this part of the contact is considered to be frictionless. The loads applied on the top of the block are shown in Figure 29. It can be noticed that at time between 1.0 and 1.1 we have to push harder because of the resistance caused by the contact of the side surface with the slab. For this problem, the node-to-segment formulation fails at time 0.66.

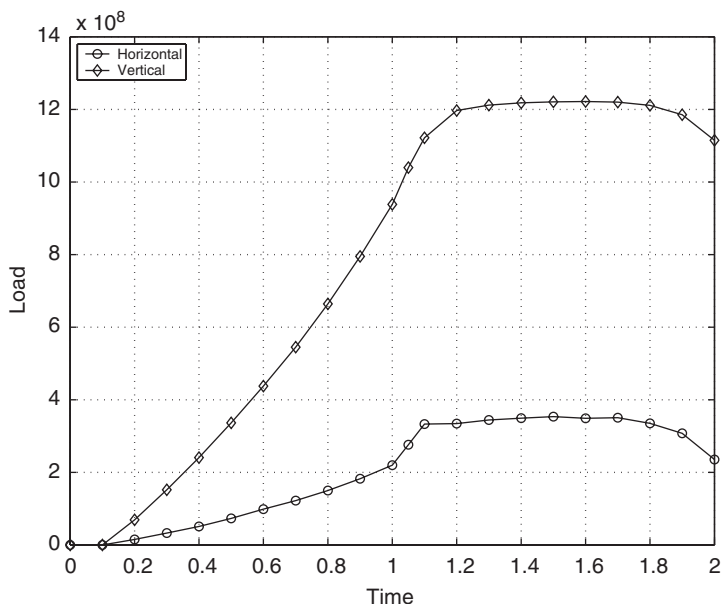


Figure 29. Computed load vs time (load parameter) curves; ironing problem.

9. CONCLUSION

A mortar finite element formulation has been proposed for the solution of large deformation frictional sliding contact problems. The implementation is demonstrated in two dimensions using linear finite elements. Extension to high order finite elements is straightforward. The solution scheme is based on a penalty regularization of mortar contact constraints and the linearization of the contact virtual work was given for solving the problem using a Newton–Raphson strategy. Several numerical examples were computed to indicate that the methodology is robust, accurate and able to pass the patch test for non-conforming meshes along the contact surface. Several non-linear problems with large deformations and sliding exhibit the superior robustness of the method when compared with traditional node to surface strategies.

The numerical results also proved that the definition of continuous normal fields is effective in overcoming difficulties in segmentation and formulation of normal contact constraints caused by non-smooth geometry inherent to the discretized contact problem. The extension of the idea to three dimensional problems is also possible and should make the algorithm more robust, although the formulation is much more involved than the two dimensional case presented here.

It is expected that future work will implement the method in three dimensional frictional contact problems. Although the idea is similar, the three dimensional case will have more challenges associated with the searching of contact segments and the linearization of the contact virtual work.

APPENDIX A: LINEARIZATION DETAILS FOR MORTAR FRICTION FORMULATION

We begin by taking the directional derivative of (30) to obtain

$$\begin{aligned} \Delta G^{cm}(\boldsymbol{\varphi}^h, \boldsymbol{\Phi}^h) = & -\sum_A \sum_B \sum_C \Delta \lambda_A \cdot \left[n_{AB}^{(1)} \boldsymbol{\Phi}_B^{*(1)} - n_{AC}^{(2)} \boldsymbol{\Phi}_C^{*(2)} \right] \\ & - \sum_A \sum_B \sum_C \lambda_A \cdot \left[\Delta n_{AB}^{(1)} \boldsymbol{\Phi}_B^{*(1)} - \Delta n_{AC}^{(2)} \boldsymbol{\Phi}_C^{*(2)} \right] \end{aligned} \quad (\text{A1})$$

As indicated in (56) and (57), the mortar coefficients are ultimately defined in terms of segment contributions. Thus, it is straightforward to express $\Delta n_{AB}^{(1)}$ and $\Delta n_{AC}^{(2)}$ in (A1) in terms of sums of segment contributions. The result is that some portions of the mortar stiffness are most conveniently written as assemblies of individual mortar segment contributions, while other portions of the stiffness involve a more intricate coupling between these segment contributions.

To specify the contact linearization, we shall proceed by linearizing the following quantities individually:

1. the normal and tangential directions defined in (51) and (52) (Section A.1);
2. the co-ordinates of the segment ends $\xi_a^{(1)}$, $\xi_b^{(1)}$, $\xi_a^{(2)}$ and $\xi_b^{(2)}$ (Section A.2);
3. the mortar integrals $n_{AB}^{(1)}$ and $n_{AC}^{(2)}$ (Section A.3); and
4. the contact traction expressions (Section A.4).

A.1. Linearization of normal and tangential vectors

Using the notation in Figure 3, we wish to linearize the normal vector at point A , which will in turn depend also on the two nodes $A-1$ and $A+1$ adjacent to A . The current position of these three points are $\boldsymbol{\varphi}_{A-1}$, $\boldsymbol{\varphi}_A$ and $\boldsymbol{\varphi}_{A+1}$, respectively. The components of $\boldsymbol{\varphi}_i$ are denoted as φ_{i_x} and φ_{i_y} .

We define two auxiliary vectors $\bar{\mathbf{n}}_{A_1}$ and $\bar{\mathbf{n}}_{A_2}$, which are outward normal vectors to the elements $(A-1) - A$ and $A - (A+1)$, as

$$\bar{\mathbf{n}}_{A_1} = \begin{bmatrix} \varphi_{A_y} - \varphi_{A-1_y} \\ -(\varphi_{A_x} - \varphi_{A-1_x}) \end{bmatrix} = \begin{bmatrix} \bar{n}_{A_x} \\ \bar{n}_{A_y} \end{bmatrix} \quad (\text{A2})$$

and

$$\bar{\mathbf{n}}_{A_2} = \begin{bmatrix} \varphi_{A+1_y} - \varphi_{A_y} \\ -(\varphi_{A+1_x} - \varphi_{A_x}) \end{bmatrix} = \begin{bmatrix} \bar{n}_{A+1_x} \\ \bar{n}_{A+1_y} \end{bmatrix} \quad (\text{A3})$$

Then, l_1 and l_2 in (51) are represented as

$$l_1 = \sqrt{\bar{\mathbf{n}}_{A_1} \cdot \bar{\mathbf{n}}_{A_1}} \quad (\text{A4})$$

and

$$l_2 = \sqrt{\bar{\mathbf{n}}_{A_2} \cdot \bar{\mathbf{n}}_{A_2}} \quad (\text{A5})$$

One may substitute (A4) and (A5) into (51) to obtain

$$\begin{aligned}\hat{\mathbf{n}}_A &= \sqrt{\bar{\mathbf{n}}_{A_2} \cdot \bar{\mathbf{n}}_{A_2}} \frac{\bar{\mathbf{n}}_{A_1}}{\sqrt{\bar{\mathbf{n}}_{A_1} \cdot \bar{\mathbf{n}}_{A_1}}} + \sqrt{\bar{\mathbf{n}}_{A_1} \cdot \bar{\mathbf{n}}_{A_1}} \frac{\bar{\mathbf{n}}_{A_2}}{\sqrt{\bar{\mathbf{n}}_{A_2} \cdot \bar{\mathbf{n}}_{A_2}}} \\ &= \frac{(\bar{\mathbf{n}}_{A_2} \cdot \bar{\mathbf{n}}_{A_2}) \bar{\mathbf{n}}_{A_1} + (\bar{\mathbf{n}}_{A_1} \cdot \bar{\mathbf{n}}_{A_1}) \bar{\mathbf{n}}_{A_2}}{\sqrt{\bar{\mathbf{n}}_{A_1} \cdot \bar{\mathbf{n}}_{A_1}} \sqrt{\bar{\mathbf{n}}_{A_2} \cdot \bar{\mathbf{n}}_{A_2}}}\end{aligned}\quad (\text{A6})$$

We can redefine $\hat{\mathbf{n}}_A$ by scaling it, and still retain the final expression for \mathbf{n}_A in (50); this redefinition makes the linearization easier. The new definition of $\hat{\mathbf{n}}_A$ is

$$\hat{\mathbf{n}}_A = \begin{bmatrix} \hat{n}_{A_x} \\ \hat{n}_{A_y} \end{bmatrix} = (\bar{\mathbf{n}}_{A_2} \cdot \bar{\mathbf{n}}_{A_2}) \bar{\mathbf{n}}_{A_1} + (\bar{\mathbf{n}}_{A_1} \cdot \bar{\mathbf{n}}_{A_1}) \bar{\mathbf{n}}_{A_2} \quad (\text{A7})$$

Its directional derivative is readily computed as

$$\begin{aligned}\Delta \hat{\mathbf{n}}_A &= 2(\bar{\mathbf{n}}_{A_2} \cdot \Delta \bar{\mathbf{n}}_{A_2}) \bar{\mathbf{n}}_{A_1} + (\bar{\mathbf{n}}_{A_2} \cdot \bar{\mathbf{n}}_{A_2}) \Delta \bar{\mathbf{n}}_{A_1} \\ &\quad + 2(\bar{\mathbf{n}}_{A_1} \cdot \Delta \bar{\mathbf{n}}_{A_1}) \bar{\mathbf{n}}_{A_2} + (\bar{\mathbf{n}}_{A_1} \cdot \bar{\mathbf{n}}_{A_1}) \Delta \bar{\mathbf{n}}_{A_2}\end{aligned}\quad (\text{A8})$$

Considering the linearization of (A2) and (A3), (A8) can finally be written in matrix form

$$\Delta \hat{\mathbf{n}}_A = \begin{bmatrix} \Delta \hat{n}_{A_x} \\ \Delta \hat{n}_{A_y} \end{bmatrix} = \hat{\mathbf{M}} \begin{bmatrix} \Delta \varphi_{A-1_x} \\ \Delta \varphi_{A-1_y} \\ \Delta \varphi_{A_x} \\ \Delta \varphi_{A_y} \\ \Delta \varphi_{A+1_x} \\ \Delta \varphi_{A+1_y} \end{bmatrix} \quad (\text{A9})$$

where $\hat{\mathbf{M}}$ is a 2×6 matrix given as

$$\hat{\mathbf{M}} = \begin{bmatrix} 2\bar{n}_{A_y} \bar{n}_{A+1_x} & l_2 + 2\bar{n}_{A_y} \bar{n}_{A+1_y} \\ -l_2 - 2\bar{n}_{A_x} \bar{n}_{A+1_x} & -2\bar{n}_{A_x} \bar{n}_{A+1_y} \\ 2\bar{n}_{A+1_y} \bar{n}_{A_x} - 2\bar{n}_{A_y} \bar{n}_{A+1_x} & 2\bar{n}_{A+1_y} \bar{n}_{A_y} - l_2 - 2\bar{n}_{A_y} \bar{n}_{A+1_y} + l_1 \\ -2\bar{n}_{A+1_x} \bar{n}_{A_x} + l_2 + 2\bar{n}_{A_x} \bar{n}_{A+1_x} - l_1 & -2\bar{n}_{A+1_x} \bar{n}_{A_y} + 2\bar{n}_{A_x} \bar{n}_{A+1_y} \\ -2\bar{n}_{A+1_y} \bar{n}_{A_x} & -2\bar{n}_{A+1_y} \bar{n}_{A_y} - l_1 \\ 2\bar{n}_{A+1_x} \bar{n}_{A_x} + l_1 & 2\bar{n}_{A+1_x} \bar{n}_{A_y} \end{bmatrix}^T \quad (\text{A10})$$

In (A10), \bar{n}_{A_x} , \bar{n}_{A_y} , \bar{n}_{A+1_x} and \bar{n}_{A+1_y} are defined in (A2) and (A3), while l_1 and l_2 are defined in (A4) and (A5).

From (50), we have the directional derivative of \mathbf{n}_A as

$$\Delta \mathbf{n}_A = \frac{\Delta \hat{\mathbf{n}}_A}{\sqrt{\hat{\mathbf{n}}_A \cdot \hat{\mathbf{n}}_A}} - \frac{(\hat{\mathbf{n}}_A \cdot \Delta \hat{\mathbf{n}}_A) \hat{\mathbf{n}}_A}{\sqrt{(\hat{\mathbf{n}}_A \cdot \hat{\mathbf{n}}_A)^3}} \quad (\text{A11})$$

One may substitute in (A8), to obtain the matrix form

$$\Delta \mathbf{n}_A = \begin{bmatrix} \Delta n_{A_x} \\ \Delta n_{A_y} \end{bmatrix} = \mathbf{M} \begin{bmatrix} \Delta \varphi_{A-1_x} \\ \Delta \varphi_{A-1_y} \\ \Delta \varphi_{A_x} \\ \Delta \varphi_{A_y} \\ \Delta \varphi_{A+1_x} \\ \Delta \varphi_{A+1_y} \end{bmatrix} \quad (\text{A12})$$

where \mathbf{M} is also a 2×6 matrix expressed as

$$\mathbf{M} = \frac{1}{\sqrt{\hat{\mathbf{n}}_A \cdot \hat{\mathbf{n}}_A}} \hat{\mathbf{M}} - \frac{1}{\sqrt{(\hat{\mathbf{n}}_A \cdot \hat{\mathbf{n}}_A)^3}} \begin{bmatrix} \hat{n}_{A_x}^2 & \hat{n}_{A_x} \hat{n}_{A_y} \\ \hat{n}_{A_x} \hat{n}_{A_y} & \hat{n}_{A_y}^2 \end{bmatrix} \hat{\mathbf{M}} \quad (\text{A13})$$

Finally, the directional derivative of the unit tangential vector can be obtained from (52) as

$$\Delta \boldsymbol{\tau}_A = \mathbf{e}_3 \times \Delta \mathbf{n}_A \quad (\text{A14})$$

A.2. Linearization of co-ordinates of the segment ends, $\xi_a^{(1)}$, $\xi_b^{(1)}$, $\xi_a^{(2)}$ and $\xi_b^{(2)}$

A segment end co-ordinate can be either an element node or the projection point of an element node. For an element node, the directional derivative of the surface co-ordinate is 0. For the projection point, the directional derivative can be computed by the linearization of (54) and (55).

Considering $\xi_a^{(1)}$, if it is a slave element node, we have

$$\Delta \xi_a^{(1)} = 0 \quad (\text{A15})$$

At the same time, the projection of $\xi_a^{(1)}$ on the master surface is $\xi_a^{(2)}$. By linearizing (54), one obtains

$$\begin{aligned} \Delta \xi_a^{(2)} = & - \frac{1}{\left[N_{1,\xi}^{(2)}(\xi_a^{(2)}) \varphi_{1_x}^{(2)} + N_{2,\xi}^{(2)}(\xi_a^{(2)}) \varphi_{2_x}^{(2)} \right] n_{1_y} - \left[N_{1,\xi}^{(2)}(\xi_a^{(2)}) \varphi_{1_y}^{(2)} + N_{2,\xi}^{(2)}(\xi_a^{(2)}) \varphi_{2_y}^{(2)} \right] n_{1_x}} \\ & \times \left\{ \left[N_1^{(2)}(\xi_a^{(2)}) \Delta \varphi_{1_x}^{(2)} + N_2^{(2)}(\xi_a^{(2)}) \Delta \varphi_{2_x}^{(2)} - \Delta \varphi_{1_x}^{(1)} \right] n_{1_y} \right. \\ & \left. - \left[N_1^{(2)}(\xi_a^{(2)}) \Delta \varphi_{1_y}^{(2)} + N_2^{(2)}(\xi_a^{(2)}) \Delta \varphi_{2_y}^{(2)} - \Delta \varphi_{1_y}^{(1)} \right] n_{1_x} \right\} \end{aligned}$$

$$\begin{aligned}
& + \left[N_1^{(2)}(\xi_a^{(2)})\varphi_{1_x}^{(2)} + N_2^{(2)}(\xi_a^{(2)})\varphi_{2_x}^{(2)} - \varphi_{1_x}^{(1)} \right] \Delta n_{1_y} \\
& - \left[N_1^{(2)}(\xi_a^{(2)})\varphi_{1_y}^{(2)} + N_2^{(2)}(\xi_a^{(2)})\varphi_{2_y}^{(2)} - \varphi_{1_y}^{(1)} \right] \Delta n_{1_x} \} \quad (A16)
\end{aligned}$$

where $(\varphi_{1_x}^{(1)}, \varphi_{1_y}^{(1)})$ is the current position of slave node denoted by $\xi_a^{(1)}$; $(\varphi_{1_x}^{(2)}, \varphi_{1_y}^{(2)})$ and $(\varphi_{2_x}^{(2)}, \varphi_{2_y}^{(2)})$ are the current positions of the two master element nodes; (n_{1_x}, n_{1_y}) denote the unit normal for the slave node $\xi_a^{(1)}$; $(\Delta n_{1_x}, \Delta n_{1_y})$ are its directional derivatives (given by (A12)); and $N_{i,\xi}^{(2)}$, $i = 1, 2$, are the partial derivatives of $N_i^{(2)}$ with respect to ξ .

On the other hand, if $\xi_a^{(1)}$ denotes a projection point of a master node, $\xi_a^{(2)}$, onto the slave element, we have

$$\Delta \xi_a^{(2)} = 0 \quad (A17)$$

and by linearization of (55), we have

$$\Delta \xi_a^{(1)} = -\frac{\text{num}}{\text{denom}} \quad (A18)$$

where

$$\begin{aligned}
\text{num} = & - \left[N_1^{(1)}(\xi_a^{(1)})\Delta n_{1_x} + N_2^{(1)}(\xi_a^{(1)})\Delta n_{2_x} \right] \left[N_1^{(1)}(\xi_a^{(1)})\varphi_{1_y}^{(1)} + N_2^{(1)}(\xi_a^{(1)})\varphi_{2_y}^{(1)} - \varphi_{2_y}^{(2)} \right] \\
& + \left[N_1^{(1)}(\xi_a^{(1)})\Delta n_{1_y} + N_2^{(1)}(\xi_a^{(1)})\Delta n_{2_y} \right] \left[N_1^{(1)}(\xi_a^{(1)})\varphi_{1_x}^{(1)} + N_2^{(1)}(\xi_a^{(1)})\varphi_{2_x}^{(1)} - \varphi_{2_x}^{(2)} \right] \\
& - \left[N_1^{(1)}(\xi_a^{(1)})n_{1_x} + N_2^{(1)}(\xi_a^{(1)})n_{2_x} \right] \left[N_1^{(1)}(\xi_a^{(1)})\Delta \varphi_{1_y}^{(1)} + N_2^{(1)}(\xi_a^{(1)})\Delta \varphi_{2_y}^{(1)} - \Delta \varphi_{2_y}^{(2)} \right] \\
& + \left[N_1^{(1)}(\xi_a^{(1)})n_{1_y} + N_2^{(1)}(\xi_a^{(1)})n_{2_y} \right] \left[N_1^{(1)}(\xi_a^{(1)})\Delta \varphi_{1_x}^{(1)} + N_2^{(1)}(\xi_a^{(1)})\Delta \varphi_{2_x}^{(1)} - \Delta \varphi_{2_x}^{(2)} \right] \quad (A19)
\end{aligned}$$

and

$$\begin{aligned}
\text{denom} = & \left[N_{1,\xi}^{(1)}(\xi_a^{(1)})n_{1_x} + N_{2,\xi}^{(1)}(\xi_a^{(1)})n_{2_x} \right] \left[N_1^{(1)}(\xi_a^{(1)})\varphi_{1_y}^{(1)} + N_2^{(1)}(\xi_a^{(1)})\varphi_{2_y}^{(1)} - \varphi_{2_y}^{(2)} \right] \\
& - \left[N_{1,\xi}^{(1)}(\xi_a^{(1)})n_{1_y} + N_{2,\xi}^{(1)}(\xi_a^{(1)})n_{2_y} \right] \left[N_1^{(1)}(\xi_a^{(1)})\varphi_{1_x}^{(1)} + N_2^{(1)}(\xi_a^{(1)})\varphi_{2_x}^{(1)} - \varphi_{2_x}^{(2)} \right] \\
& + \left[N_1^{(1)}(\xi_a^{(1)})n_{1_x} + N_2^{(1)}(\xi_a^{(1)})n_{2_x} \right] \left[N_{1,\xi}^{(1)}(\xi_a^{(1)})\varphi_{1_y}^{(1)} + N_{2,\xi}^{(1)}(\xi_a^{(1)})\varphi_{2_y}^{(1)} \right] \\
& - \left[N_1^{(1)}(\xi_a^{(1)})n_{1_y} + N_2^{(1)}(\xi_a^{(1)})n_{2_y} \right] \left[N_{1,\xi}^{(1)}(\xi_a^{(1)})\varphi_{1_x}^{(1)} + N_{2,\xi}^{(1)}(\xi_a^{(1)})\varphi_{2_x}^{(1)} \right] \quad (A20)
\end{aligned}$$

In (A20), (n_{1x}, n_{1y}) and (n_{2x}, n_{2y}) are unit normal vectors at the two slave nodes; $(\varphi_{2x}^{(2)}, \varphi_{2y}^{(2)})$ define the current position of the master point denoted by $\xi_a^{(2)}$; and $(\varphi_{1x}^{(1)}, \varphi_{1y}^{(1)})$ and $(\varphi_{2x}^{(1)}, \varphi_{2y}^{(1)})$ are the current positions of the two slave element nodes.

In a directly analogous manner to what is given above, we can compute $\Delta\xi_b^{(1)}$ and $\Delta\xi_b^{(2)}$.

A.3. Linearization of $n_{AB}^{(1)}$ and $n_{AC}^{(2)}$

Recalling that $n_{AB}^{(1)}$ and $n_{AC}^{(2)}$ are summations of segment contributions, we will obtain their linearizations by linearizing segment contributions and then assembling the results.

The geometry on the slave side of a mortar segment is parameterized via

$$\boldsymbol{\varphi}^{(1)} = N_1^{(1)}(\xi^{(1)})\boldsymbol{\varphi}_1^{(1)} + N_2^{(1)}(\xi^{(1)})\boldsymbol{\varphi}_2^{(1)} \quad (\text{A21})$$

where

$$\begin{aligned} N_1 &= \frac{1}{2}(1 - \xi) \\ N_2 &= \frac{1}{2}(1 + \xi) \end{aligned} \quad (\text{A22})$$

By recalling the parameterization given in (58), one can write J_{seg} in (63) as

$$J_{\text{seg}} = \frac{1}{4} \sqrt{(\boldsymbol{\varphi}_2^{(1)} - \boldsymbol{\varphi}_1^{(1)}) \cdot (\boldsymbol{\varphi}_2^{(1)} - \boldsymbol{\varphi}_1^{(1)}) (\xi_b^{(1)} - \xi_a^{(1)})} \quad (\text{A23})$$

The directional derivatives of $n_{AB}^{(1)\text{seg}}$ and $n_{AC}^{(2)\text{seg}}$ in (61) and (62) are:

$$\begin{aligned} \Delta n_{AB}^{(1)\text{seg}} &= \sum_{g=1}^{ng} \left[\Delta J_{\text{seg}} w_g N_A^{(1)}(\xi_g^{(1)}) N_B^{(1)}(\xi_g^{(1)}) \right] \\ &\quad + \sum_{g=1}^{ng} \left[J_{\text{seg}} w_g \Delta(N_A^{(1)}(\xi_g^{(1)})) N_B^{(1)}(\xi_g^{(1)}) \right] \\ &\quad + \sum_{g=1}^{ng} \left[J_{\text{seg}} w_g N_A^{(1)}(\xi_g^{(1)}) \Delta(N_B^{(1)}(\xi_g^{(1)})) \right] \end{aligned} \quad (\text{A24})$$

and

$$\begin{aligned} \Delta n_{AC}^{(2)\text{seg}} &= \sum_{g=1}^{ng} \left[\Delta J_{\text{seg}} w_g N_A^{(1)}(\xi_g^{(1)}) N_C^{(2)}(\xi_g^{(2)}) \right] \\ &\quad + \sum_{g=1}^{ng} \left[J_{\text{seg}} w_g \Delta(N_A^{(1)}(\xi_g^{(1)})) N_C^{(2)}(\xi_g^{(2)}) \right] \\ &\quad + \sum_{g=1}^{ng} \left[J_{\text{seg}} w_g N_A^{(1)}(\xi_g^{(1)}) \Delta(N_C^{(2)}(\xi_g^{(2)})) \right] \end{aligned} \quad (\text{A25})$$

We can compute ΔJ_{seg} , $\Delta(N_{A/B}^{(1)}(\xi_g^{(1)}))$ and $\Delta(N_C^{(2)}(\xi_g^{(2)}))$ via

$$\begin{aligned} \Delta J_{\text{seg}} &= \frac{1}{4} \sqrt{(\boldsymbol{\varphi}_2^{(1)} - \boldsymbol{\varphi}_1^{(1)}) \cdot (\boldsymbol{\varphi}_2^{(1)} - \boldsymbol{\varphi}_1^{(1)})} (\Delta \xi_b^{(1)} - \Delta \xi_a^{(1)}) \\ &\quad + \frac{1}{4} (\xi_b^{(1)} - \xi_a^{(1)}) \frac{(\boldsymbol{\varphi}_2^{(1)} - \boldsymbol{\varphi}_1^{(1)}) \cdot (\Delta \boldsymbol{\varphi}_2^{(1)} - \Delta \boldsymbol{\varphi}_1^{(1)})}{\sqrt{(\boldsymbol{\varphi}_2^{(1)} - \boldsymbol{\varphi}_1^{(1)}) \cdot (\boldsymbol{\varphi}_2^{(1)} - \boldsymbol{\varphi}_1^{(1)})}} \end{aligned} \quad (\text{A26})$$

$$\Delta N_{A/B}^{(1)}(\xi_g^{(1)}) = N_{A/B, \xi}^{(1)} \Delta \xi_g^{(1)} = \frac{1}{2} (1 - \eta_g) N_{A/B, \xi}^{(1)} \Delta \xi_a^{(1)} + \frac{1}{2} (1 + \eta_g) N_{A/B, \xi}^{(1)} \Delta \xi_b^{(1)} \quad (\text{A27})$$

and

$$\Delta N_C^{(2)}(\xi_g^{(2)}) = N_{C, \xi}^{(2)} \Delta \xi_g^{(2)} = \frac{1}{2} (1 - \eta_g) N_{C, \xi}^{(2)} \Delta \xi_a^{(2)} + \frac{1}{2} (1 + \eta_g) N_{C, \xi}^{(2)} \Delta \xi_b^{(2)} \quad (\text{A28})$$

One may substitute (A26), (A27) and (A28) into (A24) and (A25) to obtain $\Delta n_{AB}^{(1) \text{ seg}}$ and $\Delta n_{AC}^{(2) \text{ seg}}$:

$$\begin{aligned} \Delta n_{AB}^{(1) \text{ seg}} &= \sum_{g=1}^{ng} \left\{ \frac{1}{2} w_g J_{\text{seg}} (1 - \eta_g) \left[N_{A, \xi}^{(1)}(\xi_g^{(1)}) N_B^{(1)}(\xi_g^{(1)}) + N_A^{(1)}(\xi_g^{(1)}) N_{B, \xi}^{(1)}(\xi_g^{(1)}) \right] \right. \\ &\quad \left. - \frac{J_{\text{seg}}}{\xi_b^{(1)} - \xi_a^{(1)}} w_g N_A^{(1)}(\xi_g^{(1)}) N_B^{(1)}(\xi_g^{(1)}) \right\} \Delta \xi_a^{(1)} \\ &\quad + \sum_{g=1}^{ng} \left\{ \frac{1}{2} w_g J_{\text{seg}} (1 + \eta_g) \left[N_{A, \xi}^{(1)}(\xi_g^{(1)}) N_B^{(1)}(\xi_g^{(1)}) + N_A^{(1)}(\xi_g^{(1)}) N_{B, \xi}^{(1)}(\xi_g^{(1)}) \right] \right. \\ &\quad \left. + \frac{J_{\text{seg}}}{\xi_b^{(1)} - \xi_a^{(1)}} w_g N_A^{(1)}(\xi_g^{(1)}) N_B^{(1)}(\xi_g^{(1)}) \right\} \Delta \xi_b^{(1)} \\ &\quad + \sum_{g=1}^{ng} \left\{ \frac{1}{4} w_g N_A^{(1)}(\xi_g^{(1)}) N_B^{(1)}(\xi_g^{(1)}) (\xi_b^{(1)} - \xi_a^{(1)}) \frac{(\boldsymbol{\varphi}_2^{(1)} - \boldsymbol{\varphi}_1^{(1)}) \cdot (\Delta \boldsymbol{\varphi}_2^{(1)} - \Delta \boldsymbol{\varphi}_1^{(1)})}{\sqrt{(\boldsymbol{\varphi}_2^{(1)} - \boldsymbol{\varphi}_1^{(1)}) \cdot (\boldsymbol{\varphi}_2^{(1)} - \boldsymbol{\varphi}_1^{(1)})}} \right\} \end{aligned} \quad (\text{A29})$$

and

$$\begin{aligned} \Delta n_{AC}^{(2) \text{ seg}} &= \sum_{g=1}^{ng} \left\{ \frac{1}{2} w_g J_{\text{seg}} (1 - \eta_g) N_{A, \xi}^{(1)}(\xi_g^{(1)}) N_C^{(2)}(\xi_g^{(2)}) \right. \\ &\quad \left. - \frac{J_{\text{seg}}}{\xi_b^{(1)} - \xi_a^{(1)}} w_g N_A^{(1)}(\xi_g^{(1)}) N_C^{(2)}(\xi_g^{(2)}) \right\} \Delta \xi_a^{(1)} \end{aligned}$$

$$\begin{aligned}
& + \sum_{g=1}^{ng} \left\{ \frac{1}{2} w_g J_{\text{seg}} (1 + \eta_g) N_{A,\xi}^{(1)}(\xi_g^{(1)}) N_C^{(2)}(\xi_g^{(2)}) \right. \\
& + \frac{J_{\text{seg}}}{\xi_b^{(1)} - \xi_a^{(1)}} w_g N_A^{(1)}(\xi_g^{(1)}) N_C^{(2)}(\xi_g^{(2)}) \left. \right\} \Delta \xi_b^{(1)} \\
& + \sum_{g=1}^{ng} \left\{ \frac{1}{2} w_g J_{\text{seg}} (1 - \eta_g) N_A^{(1)}(\xi_g^{(1)}) N_{C,\xi}^{(2)}(\xi_g^{(2)}) \right\} \Delta \xi_a^{(2)} \\
& + \sum_{g=1}^{ng} \left\{ \frac{1}{2} w_g J_{\text{seg}} (1 + \eta_g) N_A^{(1)}(\xi_g^{(1)}) N_{C,\xi}^{(2)}(\xi_g^{(2)}) \right\} \Delta \xi_b^{(2)} \\
& + \sum_{g=1}^{ng} \left\{ \frac{1}{4} w_g N_A^{(1)}(\xi_g^{(1)}) N_C^{(2)}(\xi_g^{(2)}) (\xi_b^{(1)} - \xi_a^{(1)}) \right. \\
& \times \left. \frac{(\boldsymbol{\phi}_2^{(1)} - \boldsymbol{\phi}_1^{(1)}) \cdot (\Delta \boldsymbol{\phi}_2^{(1)} - \Delta \boldsymbol{\phi}_1^{(1)})}{\sqrt{(\boldsymbol{\phi}_2^{(1)} - \boldsymbol{\phi}_1^{(1)}) \cdot (\boldsymbol{\phi}_2^{(1)} - \boldsymbol{\phi}_1^{(1)})}} \right\} \quad (\text{A30})
\end{aligned}$$

Substituting directional derivatives of $\xi_a^{(1)}$, $\xi_a^{(2)}$, $\xi_b^{(1)}$ and $\xi_a^{(2)}$ into (A29) and (A30) and summing the segment contributions gives the linearization of $n_{AB}^{(1)}$ and $n_{AC}^{(2)}$.

A.4. Linearization of contact traction

The final intermediate result is the specification of the contact traction linearizations. We assume a penalty treatment of these, although similar expressions for augmented Lagrangian treatments are readily obtained.

A.4.1. Normal traction. One may compute the directional derivative of the normal traction defined in (38) as

$$\Delta \boldsymbol{\lambda}_{N_A} = -\varepsilon_N H(g_A) \Delta g_A \mathbf{n}_A - \varepsilon_N \langle g_A \rangle \Delta \mathbf{n}_A \quad (\text{A31})$$

Computing the directional derivative of g_A in (36), and substituting into (A31) gives

$$\begin{aligned}
\Delta \boldsymbol{\lambda}_{N_A} = & -\varepsilon_N \kappa_A H(g_A) \left\{ \Delta \mathbf{n}_A \cdot \left[\sum_B n_{AB}^{(1)} \boldsymbol{\phi}_B^{(1)} - \sum_C n_{AC}^{(2)} \boldsymbol{\phi}_C^{(2)} \right] \right. \\
& + \mathbf{n}_A \cdot \left[\sum_B \left(\Delta n_{AB}^{(1)} \boldsymbol{\phi}_B^{(1)} + n_{AB}^{(1)} \Delta \boldsymbol{\phi}_B^{(1)} \right) - \sum_C \left(\Delta n_{AC}^{(2)} \boldsymbol{\phi}_C^{(2)} + n_{AC}^{(2)} \Delta \boldsymbol{\phi}_C^{(2)} \right) \right] \left. \right\} \mathbf{n}_A \\
& - \varepsilon_N \langle g_A \rangle \Delta \mathbf{n}_A \quad (\text{A32})
\end{aligned}$$

where the results from the preceding subsections are substituted in the appropriate locations.

A.4.2. Frictional traction. From (49), we can compute the directional derivative of frictional traction

$$\Delta \lambda_{T_{A_{n+1}}} = \begin{cases} \Delta \lambda_{T_{A_{n+1}}}^{\text{trial}} \tau_A + \lambda_{T_{A_{n+1}}}^{\text{trial}} \Delta \tau_A & \text{if } (\Phi_{n+1}^{\text{trial}}) \leq 0, \text{ stick} \\ \mu \Delta \|\lambda_{N_A}\| \tau_A + \mu \|\lambda_{N_A}\| \Delta \tau_A & \text{otherwise, slip} \end{cases} \quad (\text{A33})$$

where $\Delta \lambda_{T_{A_{n+1}}}^{\text{trial}}$ can be computed from (47) as

$$\begin{aligned} \Delta \lambda_{T_{A_{n+1}}}^{\text{trial}} = & -\varepsilon_T \kappa_A \Delta \tau_A \cdot \left[\sum_C \left(n_{AC_{n+1}}^{(2)} - n_{AC_n}^{(2)} \right) \Phi_C^{(2)} - \sum_B \left(n_{AB_{n+1}}^{(1)} - n_{AB_n}^{(1)} \right) \Phi_B^{(1)} \right] \\ & -\varepsilon_T \kappa_A \tau_A \cdot \left\{ \sum_C \left[\Delta n_{AC}^{(2)} \Phi_C^{(2)} + \left(n_{AC_{n+1}}^{(2)} - n_{AC_n}^{(2)} \right) \Delta \Phi_C^{(2)} \right] \right. \\ & \left. - \sum_B \left[\Delta n_{AB}^{(1)} \Phi_B^{(1)} + \left(n_{AB_{n+1}}^{(1)} - n_{AB_n}^{(1)} \right) \Delta \Phi_B^{(1)} \right] \right\} \end{aligned} \quad (\text{A34})$$

A.5. Assembly of the contact stiffness

In summarizing this process, we assume that all nodes associated with the mortar operator are ordered via

$$\Phi = \begin{bmatrix} \Phi_1^{(1)} \\ \Phi_2^{(1)} \\ \vdots \\ \Phi_{ns}^{(1)} \\ \Phi_1^{(2)} \\ \Phi_2^{(2)} \\ \vdots \\ \Phi_{nm}^{(2)} \end{bmatrix} \quad (\text{A35})$$

Thus, the variations and incremental motions of all nodes can be given via

$$\delta \Phi = \begin{bmatrix} \Phi_1^{*(1)} \\ \Phi_2^{*(1)} \\ \vdots \\ \Phi_{ns}^{*(1)} \\ \Phi_1^{*(2)} \\ \Phi_2^{*(2)} \\ \vdots \\ \Phi_{nm}^{*(2)} \end{bmatrix} \quad \Delta \Phi = \begin{bmatrix} \Delta \Phi_1^{(1)} \\ \Delta \Phi_2^{(1)} \\ \vdots \\ \Delta \Phi_{ns}^{(1)} \\ \Delta \Phi_1^{(2)} \\ \Delta \Phi_2^{(2)} \\ \vdots \\ \Delta \Phi_{nm}^{(2)} \end{bmatrix} \quad (\text{A36})$$

The linearization of contact virtual work in (A1) can be written in the form of summation of direct and geometric portions as

$$\Delta G^{cm}(\Phi^h, \Phi^h) = \Delta G^{cm, \text{dir}}(\Phi^h, \Phi^h) + \Delta G^{cm, \text{geom}}(\Phi^h, \Phi^h) = \delta \Phi^T \mathbf{K}^{cm} \Delta \Phi \quad (\text{A37})$$

where

$$\Delta G^{cm, \text{dir}} = - \sum_A \sum_B \sum_C \Delta \lambda_A \cdot \left[n_{AB}^{(1)} \Phi_B^{*(1)} - n_{AC}^{(2)} \Phi_C^{*(2)} \right] = \delta \Phi^T \mathbf{K}^{cm, \text{dir}} \Delta \Phi \quad (\text{A38})$$

and

$$\Delta G^{cm, \text{geom}} = - \sum_A \sum_B \sum_C \lambda_A \cdot \left[\Delta n_{AB}^{(1)} \Phi_B^{*(1)} - \Delta n_{AC}^{(2)} \Phi_C^{*(2)} \right] = \delta \Phi^T \mathbf{K}^{cm, \text{geom}} \Delta \Phi \quad (\text{A39})$$

where \mathbf{K}^{cm} , $\mathbf{K}^{cm, \text{dir}}$ and $\mathbf{K}^{cm, \text{geom}}$ are the contact stiffness, the direct portion of the stiffness, and the geometric portion of the stiffness, respectively.

Considering the direct portion of the stiffness first, the directional derivative of λ_A can be represented as

$$\Delta \lambda_A = \mathbf{G}_A \Delta \Phi \quad (\text{A40})$$

where \mathbf{G}_A is a $2 \times 2 \cdot (ns + nm)$ matrix. Part of \mathbf{G}_A is assembled from segment contributions and another part of it is assembled from nodal contributions. When we assemble \mathbf{G}_A , we split it into two parts. One is from the normal contribution and the other is from the frictional contribution, i.e.

$$\begin{aligned} \Delta \lambda_A &= \Delta \lambda_{A_N} + \Delta \lambda_{A_T} = \mathbf{G}_A \Delta \Phi \\ &= \mathbf{G}_{A_N} \Delta \Phi + \mathbf{G}_{A_T} \Delta \Phi \end{aligned} \quad (\text{A41})$$

where \mathbf{G}_{A_N} and \mathbf{G}_{A_T} are extracted from equations (A32) and (A33). For example, considering the normal operator for the kinematically linear case, the directional derivatives of the normal

vectors \mathbf{n}_A and the mortar projection operators $n_{AB}^{(i)}$ disappear from (A32), and the expression for \mathbf{G}_{AN} extracted from it becomes

$$\mathbf{G}_{AN}|_{\text{kin.linear}} = -\varepsilon_N \kappa_A H(g_A) \begin{bmatrix} n_{Ax} n_{Ax} & n_{Ax} n_{Ay} \\ n_{Ay} n_{Ax} & n_{Ay} n_{Ay} \end{bmatrix} \begin{bmatrix} n_{A1}^{(1)} \mathbf{I} & n_{A2}^{(1)} \mathbf{I} & \dots & n_{A1}^{(2)} \mathbf{I} & n_{A2}^{(2)} \mathbf{I} & \dots \end{bmatrix} \quad (\text{A42})$$

where n_{Ax} and n_{Ay} are the x and y components of the normal vector \mathbf{n}_A . \mathbf{I} is the 2×2 identity matrix. Of course, the vast majority of the elements of \mathbf{G}_A in (A42) are zero, so that in fact only the non-zero components are computed and then assembled as is described next.

After compute \mathbf{G}_A for each slave nodes, we combine them into a matrix \mathbf{G} , which is defined as

$$\mathbf{G} = \begin{bmatrix} \mathbf{G}_1 \\ \mathbf{G}_2 \\ \vdots \\ \mathbf{G}_{ns} \end{bmatrix} \quad (\text{A43})$$

which is a $2 \cdot ns \times 2 \cdot (ns + nm)$ matrix. Then the direct portion of the stiffness can be expressed as

$$\mathbf{K}^{cm, \text{dir}} = \begin{bmatrix} \hat{\mathbf{N}}^T \\ \mathbf{N}^T \end{bmatrix} \mathbf{G} \quad (\text{A44})$$

where

$$\hat{\mathbf{N}} = \begin{bmatrix} n_{11}^{(1)} \mathbf{I} & n_{12}^{(1)} \mathbf{I} & \dots \\ n_{21}^{(1)} \mathbf{I} & n_{21}^{(1)} \mathbf{I} & \dots \\ \vdots & \vdots & \vdots \end{bmatrix} \quad (\text{A45})$$

and

$$\mathbf{N} = \begin{bmatrix} n_{11}^{(2)} \mathbf{I} & n_{12}^{(2)} \mathbf{I} & \dots \\ n_{21}^{(2)} \mathbf{I} & n_{21}^{(2)} \mathbf{I} & \dots \\ \vdots & \vdots & \vdots \end{bmatrix} \quad (\text{A46})$$

In the above, $\hat{\mathbf{N}}$ is a $2 \cdot ns \times 2 \cdot ns$ matrix, \mathbf{N} is a $2 \cdot ns \times 2 \cdot nm$ matrix, and \mathbf{I} is the 2×2 identity matrix. As shown in Equation (A44), in the implementation of the direct stiffness, \mathbf{G} must be assembled first, then the multiplication is done after this assembly to get the direct stiffness $\mathbf{K}^{cm, \text{dir}}$.

The geometric contact stiffness $\mathbf{K}^{cm, \text{geom}}$ can be assembled directly from the segment contributions, according to (A39).

ACKNOWLEDGEMENTS

T. Laursen's work on this project was supported in part by the Air Force Office of Scientific Research under Contract F49620-02-1-0094, while Bin Yang was supported by Sandia National Laboratories under Contract 21757. Both sources of support are gratefully acknowledged.

REFERENCES

1. Bernardi C, Maday Y, Patera AT. A new nonconforming approach to domain decomposition: The mortar element method. In *Nonlinear Partial Differential Equations and Their Applications*, Brezia H, Lions JL (eds). Pitman: London, Wiley: New York, 1992; 13–51.
2. Wohlmuth BI. *Discretization Methods and Iterative Solvers Based on Domain Decomposition*. Springer-Verlag: Heidelberg, 2001.
3. Hallquist JO, Goudreau GL, Benson DJ. Sliding interfaces with contact-impact in large-scale lagrangian computations. *Computer Methods in Applied Mechanics and Engineering* 1985; **51**:107–137.
4. Benson DJ, Hallquist JO. A single surface contact algorithm for the post-buckling analysis of shell structures. *Computer Methods in Applied Mechanics and Engineering* 1990; **78**:141–163.
5. Wriggers P, Simo JC. A note on tangent stiffness for fully nonlinear contact problems. *Communications in Applied Numerical Methods* 1985; **1**:199–203.
6. Papadopoulos P, Taylor RL. A mixed formulation for the finite element solution of contact problems. *Computer Methods in Applied Mechanics and Engineering* 1992; **94**:373–389.
7. Laursen TA. *Computational Contact and Impact Mechanics*. Springer: Berlin, 2002.
8. Hild P. Numerical implementation of two nonconforming finite element methods for unilateral contact. *Computer Methods in Applied Mechanics and Engineering* 2000; **184**:99–123.
9. Belgacem FB, Maday Y. A spectral element methodology tuned to parallel implementations. *Computer Methods in Applied Mechanics and Engineering* 1994; **116**:59–67.
10. Belhachmi Z, Bernardi C. Resolution of fourth order problems by the mortar element method. *Computer Methods in Applied Mechanics and Engineering* 1994; **116**:53–58.
11. Maday Y, Mavriplis C, Patera AT. Nonconforming mortar element methods: application to spatial discretization. In *Domain Decomposition Methods*, SIAM: Philadelphia, 1989; 392–418.
12. Belgacem FB, Hild P, Laborde P. Approximation of the unilateral contact problem by the mortar finite element method. *Comptes Rendus De L'Academie Des Sciences* 1997; **324**:123–127.
13. Belgacem FB, Hild P, Laborde P. The mortar finite element method for contact problems. *Mathematical and Computer Modeling* 1998; **28**:263–271.
14. McDevitt TW, Laursen TA. A mortar-finite element formulation for frictional contact problems. *International Journal for Numerical Methods in Engineering* 2000; **48**:1525–1547.
15. Krause RH, Wohlmuth BI. A dirichlet-neumann type algorithm for contact problems with friction. *Technical Report*, Universitat Augsburg, 2001.
16. Wriggers P, Vu Van T, Stein E. Finite element formulation of large deformation impact-contact problems with friction. *Computers and Structures* 1990; **37**:319–331.
17. Laursen TA, Simo JC. A continuum-based finite element formulation for the implicit solution of multibody, large deformation frictional contact problems. *International Journal for Numerical Methods in Engineering* 1993; **36**:3451–3485.
18. Puso MA, Laursen TA. A mortar segment-to-segment contact method for large deformation solid mechanics. *Computer Methods in Applied Mechanics and Engineering* 2004; **129**:601–629.
19. Simo JC, Wriggers P, Taylor RL. A perturbed lagrangian formulation for the finite element solution of contact problems. *Computer Methods in Applied Mechanics and Engineering* 1985; **50**:163–180.
20. Johnson KL. *Contact Mechanics*. Cambridge University Press: Cambridge, 1985.